iScience

CellPress
OPEN ACCESS

Article

A series of xanthenes inhibiting Rad6 function and Rad6-Rad18 interaction in the PCNA ubiquitination cascade

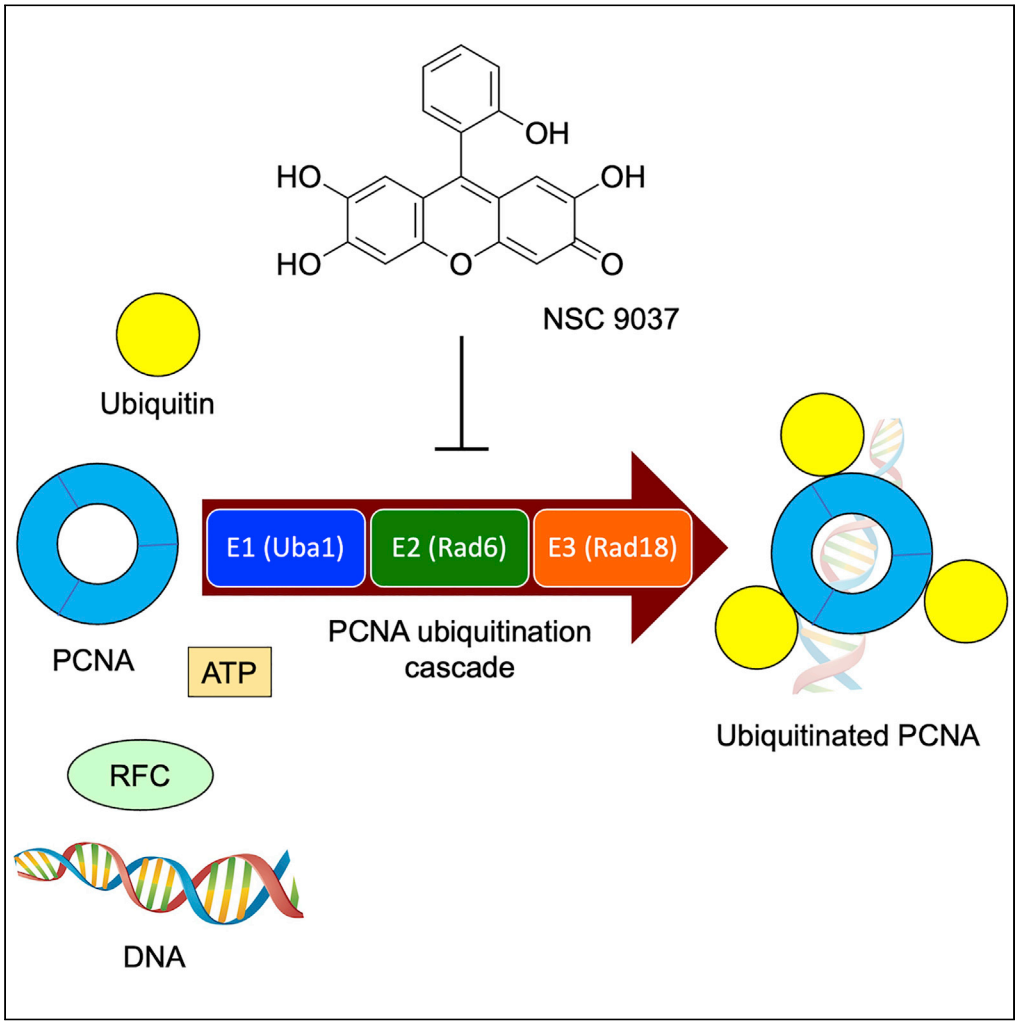

Gabriel Fenteany, Gaurav Sharma, Paras Gaur, Attila Borics, Edit Wéber, Ernő Kiss, Lajos Haracska

fenteany.gabriel@med.u-szeged.hu (G.F.)
haracska.lajos@brc.hu (L.H.)

Highlights

Alpha-based HTS for PCNA ubiquitination modulators

Target-based characterization of hits

A series of xanthenes that inhibit Rad6 functions and Rad6–Rad18 interaction

Fenteany et al., iScience *25*, 104053
April 15, 2022
https://doi.org/10.1016/j.isci.2022.104053

iScience

CellPress
OPEN ACCESS

Article

A series of xanthenes inhibiting Rad6 function and Rad6-Rad18 interaction in the PCNA ubiquitination cascade

Gabriel Fenteany,[1,7,9,*] Gaurav Sharma,[2,3,9] Paras Gaur,[2,8] Attila Borics,[4] Edit Wéber,[5] Ernő Kiss,[1] and Lajos Haracska[2,6,10,*]

SUMMARY

Ubiquitination of proliferating cell nuclear antigen (PCNA) triggers pathways of DNA damage tolerance, including mutagenic translesion DNA synthesis, and comprises a cascade of reactions involving the E1 ubiquitin-activating enzyme Uba1, the E2 ubiquitin-conjugating enzyme Rad6, and the E3 ubiquitin ligase Rad18. We report here the discovery of a series of xanthenes that inhibit PCNA ubiquitination, Rad6∼ubiquitin thioester formation, and the Rad6–Rad18 interaction. Structure-activity relationship experiments across multiple assays reveal chemical and structural features important for different activities along the pathway to PCNA ubiquitination. The compounds that inhibit these processes are all a subset of the xanthen-3-ones we tested. These small molecules thus represent first-in-class probes of Rad6 function and the association of Rad6 and Rad18, the latter being a new inhibitory activity discovered for a small molecule, in the PCNA ubiquitination cascade and potential therapeutic agents to contain cancer progression.

INTRODUCTION

Posttranslational modification of proteins through ubiquitination controls not only protein degradation by the proteasome but also a myriad of other processes. Ubiquitin and related ubiquitin-like proteins (UBLs) serve as tags and docking sites for interactions with other proteins and the formation of large protein complexes that regulate a staggering array of physiological phenomena. Modulating various steps of ubiquitination and UBL posttranslational modification pathways with small-molecule inhibitors or activators/enhancers has considerable research and therapeutic potential. One role of ubiquitin and UBLs is in the dynamic control of the DNA repair and damage tolerance machinery by affecting the function of proliferating cell nuclear antigen (PCNA), a homotrimeric sliding clamp critical for DNA replication and repair that is essentially the core around which DNA replication, repair proteins, and regulatory proteins assemble into different large complexes (reviewed in Choe and Moldovan, 2017; Dieckman et al., 2012; Fan et al., 2020; Kanao and Masutani, 2017; Knobel and Marti, 2011; Leung et al., 2018; Slade, 2018; Zafar and Eoff, 2017). DNA damage tolerance pathways evolved to circumvent the fact that DNA sites altered by chemical insult, oxidation, or photodamage that have not been repaired by other DNA repair mechanisms (such as base and nucleotide excision or mismatch repair) cause the stalling of the DNA replication fork. There are three known pathways of DNA damage tolerance: (1) translesion DNA synthesis (TLS) (reviewed in Saha et al., 2020; Vaisman and Woodgate, 2017; Yang and Gao, 2018), (2) homologous recombination-related template switching (reviewed in (Branzei and Szakal, 2017, 2016; Prado, 2018), and (3) the salvage pathway, another recombination-based pathway that has only more recently come to be appreciated (reviewed in (Branzei and Szakal, 2017, 2016; Prado, 2018). TLS is inherently prone to introducing point mutations, whereas the latter two pathways are considered error-free, although they can result in genomic rearrangements. DNA damage tolerance can thus lead to genetic alterations, oncogenesis, formation of secondary tumors after treatment with DNA-damaging agents, drug resistance, and other pathologies.

The ubiquitination of PCNA on a specific lysine residue (K164) is a key step in the activation of the DNA damage tolerance pathways. PCNA binds and coordinates the activities of myriad proteins, including DNA polymerases and other replication, repair, and regulatory factors. Once loaded onto DNA via the ATP-dependent replication factor C (RFC), PCNA can be monoubiquitinated by the E2 ubiquitin-conjugating enzyme Rad6 in complex with

[1]Institute of Genetics, Biological Research Centre, 6726 Szeged, Hungary

[2]HCEMM-BRC Mutagenesis and Carcinogenesis Research Group, Institute of Genetics, Biological Research Centre, 6726 Szeged, Hungary

[3]Doctoral School of Biology, Faculty of Science and Informatics, University of Szeged, 6726 Szeged, Hungary

[4]Laboratory of Chemical Biology, Institute of Biochemistry, Biological Research Centre, 6726 Szeged, Hungary

[5]Department of Medical Chemistry, University of Szeged, 6720, Szeged, Hungary

[6]Delta Bio 2000 Ltd., 6726 Szeged, Hungary

[7]Present address: Department of Medical Chemistry, University of Szeged, 6720 Szeged, Hungary

[8]Present address: Carver College of Medicine, University of Iowa, Iowa City IA 52242, USA

[9]These authors contributed equally

[10]Lead contact

*Correspondence: fenteany.gabriel@med.u-szeged.hu (G.F.), haracska.lajos@brc.hu (L.H.)

https://doi.org/10.1016/j.isci.2022.104053

the E3 ubiquitin ligase Rad18, the former being the catalyst and the latter the adaptor for specific substrate recognition.

The ubiquitination reaction cascade begins with ATP-dependent activation of the carboxy terminus of ubiquitin, catalyzed by the E1 ubiquitin-activating enzyme Uba1 through the formation of a ubiquitin adenylate intermediate that reacts with a specific cysteine residue on Uba1, yielding a high-energy Uba1-~ubiquitin thioester conjugate. The ubiquitin moiety is subsequently transferred to Rad6 to generate a Rad6~ubiquitin thioester conjugate, which then reacts with the side-chain amine of K164 on PCNA to form a more stable PCNA-ubiquitin isopeptide amide bond.

Monoubiquitination of PCNA triggers the TLS pathway, with the exchange of replicative DNA polymerases, which cannot copy damaged DNA, for more error-prone TLS polymerases (possessing relatively nonselective and open active sites and lacking proofreading 3′→5′ exonuclease activity) that can replicate across the DNA lesion and are considered promising cancer chemotherapeutic targets (reviewed in Saha et al., 2020; Vaisman and Woodgate, 2017; Yang and Gao, 2018). Further polyubiquitination of this ubiquitin moiety on PCNA is also possible and initiates an alternative pathway of template switching (reviewed in (Branzei and Szakal, 2017, 2016; Prado, 2018). Polyubiquitination of PCNA involves the heterodimeric E2 complex Mms2-Ubc13 and the E3 proteins HLTF or SHPRH; the polyubiquitin chain forms on ubiquitin's K63 residue rather than K48, the former type triggering template switching and the latter recognition and degradation by the proteasome (reviewed in Gallo and Brown, 2019; Kanao and Masutani, 2017; Leung et al., 2018; Ripley et al., 2020; Wilkinson et al., 2020). What determines the "decision" of whether PCNA is simply monoubiquitinated or further polyubiquitinated with activation of TLS or template switching, respectively, is unclear. In contrast, initiation of the salvage pathway is independent of PCNA ubiquitination (reviewed in (Branzei and Szakal, 2017, 2016; Prado, 2018).

The K164 residue is the main site on PCNA ubiquitinated by the Rad6–Rad18 complex, as K164R mutant PCNA is not appreciably ubiquitinated by Rad6–Rad18 (Haracska et al., 2006; Unk et al., 2008). There is some evidence, however, that two other sites, K168 (Jiang et al., 2019; Park et al., 2014; Xu et al., 2010a) and K248 (Povlsen et al., 2012), can also be modified by ubiquitin and UBLs. Rad18 itself can also be autoubiquitinated on multiple sites *in vitro* and in the cell, which seems to affect its function, subcellular localization, and stability (Miyase et al., 2005; Zeman et al., 2014).

Over a hundred proteins are known to interact with PCNA, and ubiquitination can control many of these interactions. Although PCNA forms complexes involved in normal processive replication (the "replisome") or TLS-based mutagenic replication (the "mutasome"), there are clearly many different specific types of such PCNA-based complexes with specialized functions. Bioactive compounds that selectively target ubiquitination or other posttranslational modification cascades involved at particular levels of a reaction series would provide invaluable tools for investigating the assembly of these different complexes, in addition to possessing considerable therapeutic potential.

There exist in humans over 600 ubiquitin-specific E3 proteins, about 40 ubiquitin-specific E2 enzymes, and only two ubiquitin-specific E1 enzymes, Uba1 and Uba6, with the former responsible for the overwhelming bulk of ubiquitin activation in the cell. Rad18 is a so-called "really interesting new gene" (RING) class E3 ubiquitin ligase, by far the largest class of E3 proteins, the others being the RING-Between-RING and HECT-domain E3 proteins, both of which, unlike RING E3 ubiquitin ligases, do not just function as adaptors but are real enzymes and themselves directly form ubiquitin thioester adducts to be attacked by the relevant lysine on target substrates.

There is growing awareness that the inhibition of DNA damage tolerance pathways in tumor cells represents a viable strategy for the development of new broad-based cancer chemotherapies (reviewed in (Altieri and Kelman, 2018; Cardano et al., 2020; Choe and Moldovan, 2017; Dieckman et al., 2012; Horsfall et al., 2020; Tonzi and Huang, 2019). Agents that block PCNA ubiquitination may inhibit the growth and viability of cancer cells, either as standalone drugs or as potentiators in combination with other cancer treatments, such as chemotherapy, radiotherapy, and targeted therapies, and would be of great value, particularly in cases of drug resistance.

In order to identify chemical modulators of different components of the PCNA ubiquitination cascade, we developed, optimized, and implemented high-throughput assays for PCNA ubiquitination (Fenteany et al., 2019, 2020), based on the powerful and quantitative amplified luminescent proximity homogeneous assay (Alpha)

technology. We have also developed and validated Alpha assays to interrogate individual steps in the overall cascade, namely, formation of the Uba1~ubiquitin thioester conjugate, formation of the Rad6~ubiquitin conjugate, and autoubiquitination of the E3 ubiquitin ligase Rad18 (Fenteany et al., 2020). We have also recently developed a Rad6–Rad18 association assay, the details of which are included herein.

Our assays are reconstituted systems consisting of the minimum necessary and sufficient components for each of the reactions. The Alpha assay for overall PCNA ubiquitination, which we have thus far employed as a primary functional screening assay, is reconstituted from the purified proteins required for the loading of PCNA onto DNA and the subsequent ubiquitination, whereas the Alpha assays for the individual discrete stages in the cascade are based on the relevant component proteins for each of those steps (Fenteany et al., 2019, 2020). Our screening systems thus allow us to rapidly evaluate effects on both overall and step-specific events in the ubiquitination cascade. We have thus far screened a number of chemical libraries, including the US National Cancer Institute (NCI)'s Developmental Therapeutics Program (DTP) Diversity Set VI, from which we identified the compound family that we herein describe as inhibitors of PCNA ubiquitination, Rad6~ubiquitin thioester formation, and the Rad6–Rad18 interaction, the last being a novel activity for a small molecule. The inhibitors reported here are a subset of the xanthen-3-ones tested, whereas other xanthen-3-ones and related compounds do not have inhibitory activity. Xanthene derivatives have been shown to have a range of medicinal properties, such as potential neuroprotective, antitumor, and antibacterial activities, among others (Ghahsare et al., 2019; Maia et al., 2021).

RESULTS

Refinement of the Alpha assay for PCNA ubiquitination

We further refined conditions for the Alpha assay for the overall PCNA ubiquitination reaction cascade from our previously described results (Fenteany et al., 2019, 2020), with the aim of further saving on materials (Figure 1). We examined again the concentrations of reagents that can also differ in efficacy from batch-to-batch, observing that we could reduce certain components further with some leeway (Figure 1 and (Fenteany et al., 2020)). We titrated/varied the concentration of biotinylated ubiquitin with the indicated post-reaction dilution factors (Figures 1A and 1B) and did similarly with FLAG-PCNA (Figures 1C and 1D), while holding other components constant according to previously determined concentrations (Fenteany et al., 2020). The high-dose hook effect, whereby too high concentrations of analytes yield lower signals, was apparent, typical of assays where the analytes can saturate their binding to the capture reagents as in Alpha assays, enzyme-linked immunosorbent assays, and indirect-detection (such as antibody-based) resonance energy transfer systems. We also again experimented with reducing the usage of beads by decreasing dilution factors, finding that 10-fold dilution again worked better than 5-fold dilution (Figures 1A–1D).

As shown in Figure 1E, we varied bead concentrations under conditions of reduced biotinylated ubiquitin and ATP. We found the assay to proceed well under the following conditions with minimal consumption of reagents, yet still yielding signal/background and signal/noise ratios that allowed for quantitation, and these are the conditions we used in the present study for testing compound activities (structures in Figure 2) against PCNA ubiquitination (Figure 3): 150 nM biotinylated ubiquitin, 50 nM FLAG-PCNA, 10 nM RFC, 2 nM nicked pUC19 DNA, 50 nM Uba1, 100 nM Rad6–Rad18 complex, and 100 μM ATP, with incubation at 25°C for 2 h, by which time the reaction sequence is virtually completed. Furthermore, although the signal in the subsequent Alpha detection was again better with 20 μg/mL donor and acceptor beads to bind the analytes (Figure 1E), we decided to generally dilute reactions in Alpha buffer containing 10 μg/mL of each bead type for the Alpha assay to reduce the usage of the expensive Alpha beads.

Development and compound effects in a Rad6–Rad18 interaction assay

We developed a Rad6–Rad18 interaction assay based on the Alpha system (Figure 4). We varied the concentration of each of the two proteins separately while holding the concentration of the other constant and found satisfactory results over a range of concentrations. We decided to use 100 nM of each protein.

Screening for inhibitors of PCNA ubiquitination

Compounds inhibiting PCNA ubiquitination were identified on the basis of analysis with a Microsoft Excel spreadsheet we prepared, wherein we transferred the data output from the plate reader into the spreadsheet, and plate quality control and hit quality metrics were calculated automatically. The plate quality control parameters calculated included signal-to-background ratio, signal-to-noise ratio, signal window, Z′

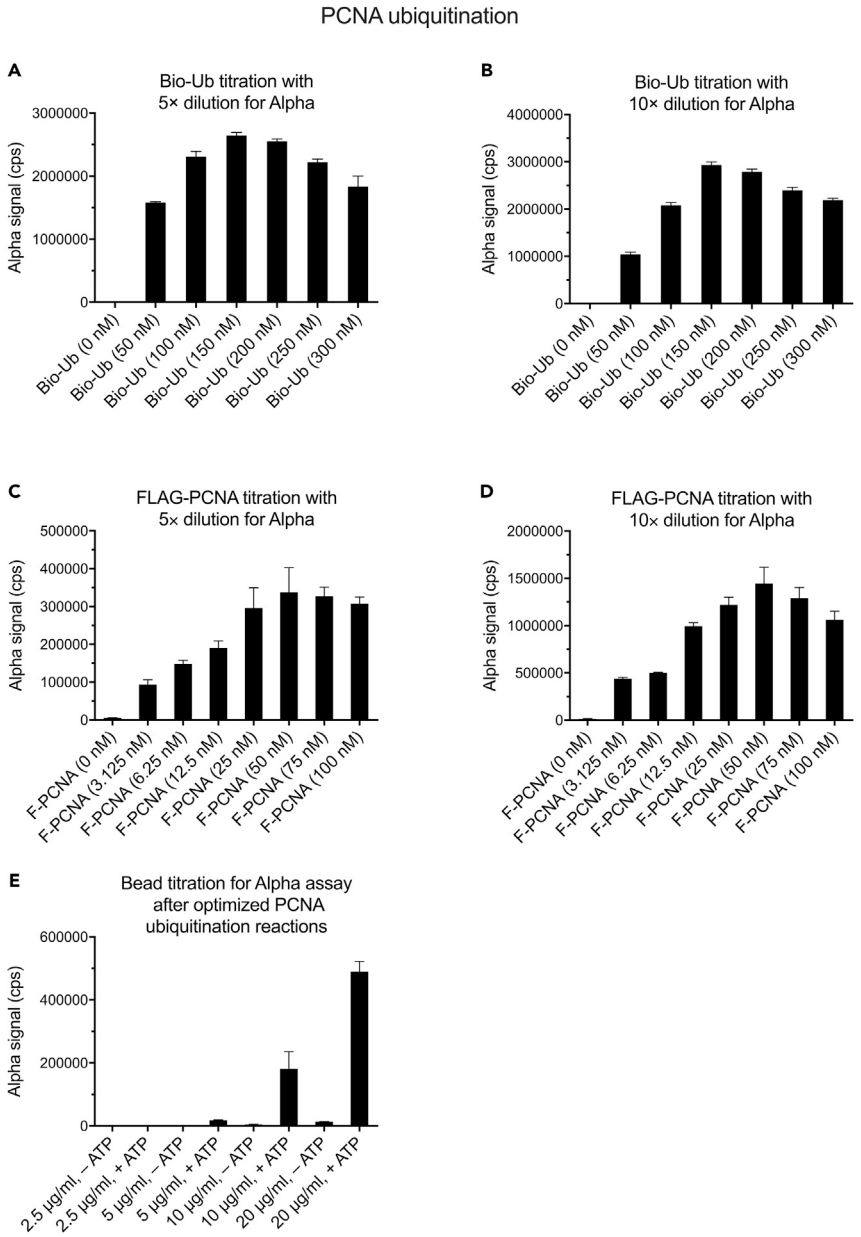

Figure 1. Refinement of the Alpha assay for the reconstituted PCNA ubiquitination reaction cascade from previously described conditions

(A) Titration of biotinylated ubiquitin against Flag-PCNA with 5-fold dilution in Alpha buffer containing 10 µg/mL donor and acceptor beads; bars represent mean with standard deviation (SD) for triplicate samples in each case.

(B) Titration of biotinylated ubiquitin against Flag-PCNA with 10-fold dilution in Alpha buffer containing 10 µg/mL donor and acceptor beads; bars represent mean with standard deviation (SD) for triplicate samples in each case.

(C) Titration of Flag-PCNA against biotinylated ubiquitin with 5-fold dilution in Alpha buffer containing 10 µg/mL donor and acceptor beads; bars represent mean with standard deviation (SD) for triplicate samples in each case.

(D) Titration of Flag-PCNA against biotinylated ubiquitin with 10-fold dilution in Alpha buffer containing 10 µg/mL donor and acceptor beads; bars represent mean with standard deviation (SD) for triplicate samples in each case.

(E) Titration of donor and acceptor bead concentrations under conditions where Bio-Ub was added to 150 nM and ATP to 100 µM with other components kept the same. Bars represent mean with standard deviation (SD) for triplicate samples in each case.

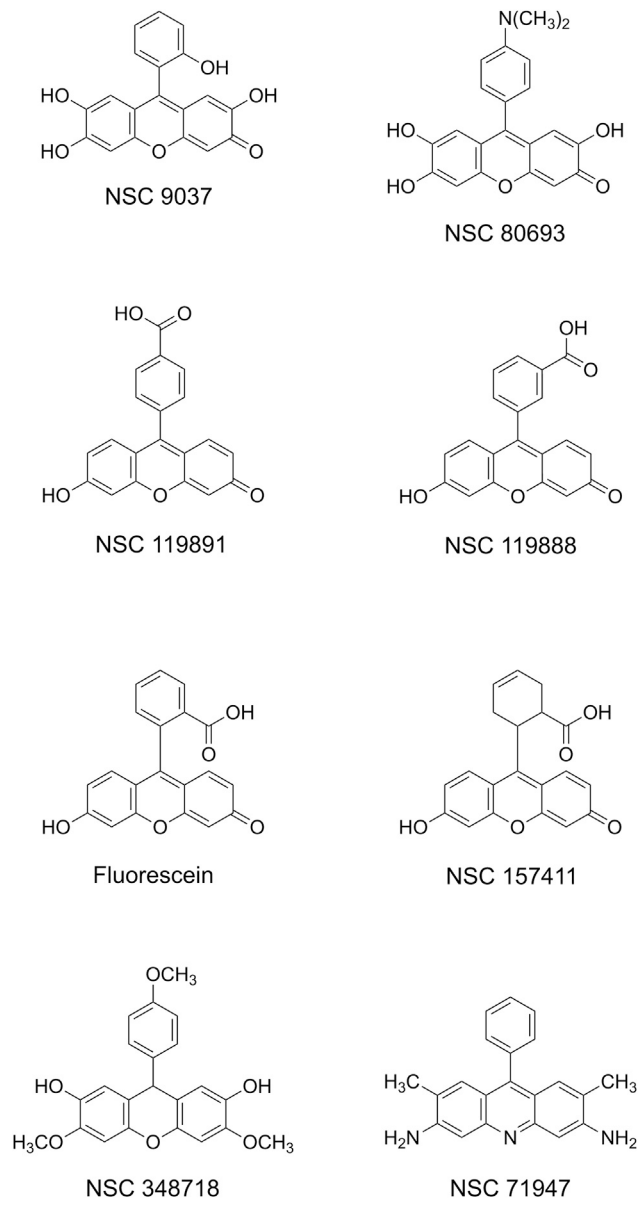

Figure 2. Structures of compounds investigated in this study

factor in both standard and robust statistical forms (calculated from positive and negative means and medians, respectively), and plate-quality strictly standardized mean difference for plate-quality assessment, both standard and robust. We typically tested compounds in triplicate on three separate plates, and if a plate was of poor quality according to the calculated metrics, additional plates were screened until there were at least three of acceptable quality (i.e., Z′ factors above 0.5).

The hit-selection parameters automatically calculated from our spreadsheets included percent normalized change in signal (experimental signal minus the mean of positive signal, with the difference divided by the mean of positive control minus the mean of negative signal), Student's t tests (in the case of replicate samples, which we generally do), *z* scores (in the case of experiments without replicates), and strictly standardized mean differences for hit selection, in both standard and robust formulations. If a compound at a high screening concentration had significant activity, it was then tested at progressively lower concentrations in serial 2-fold dilutions, with the most active compounds selected with each concentration round. The highest concentration for screening was 10 μM or 100 μM depending on stock compound plate concentration

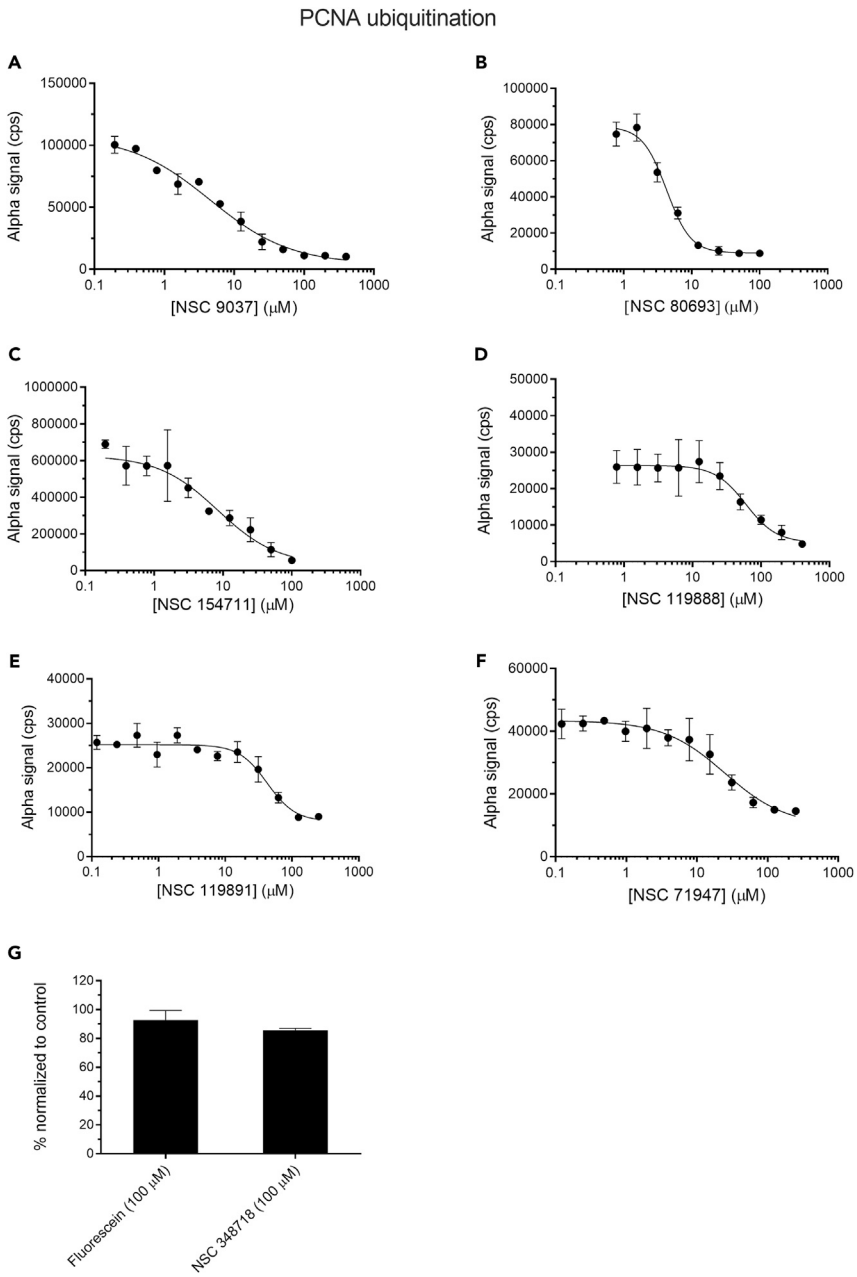

Figure 3. Dose response for PCNA ubiquitination in the presence of compounds by alpha assay

(A) Dose response of NSC 9037 for PCNA ubiquitination.

(B) Dose response of NSC 80693 for PCNA ubiquitination.

(C) Dose response of NSC 154711 for PCNA ubiquitination.

(D) Dose response of NSC 119888 for PCNA ubiquitination.

(E) Dose response of NSC 119891 for PCNA ubiquitination.

(F) Dose response of NSC 71947 for PCNA ubiquitination.

Curves in (A)-(F) were fitted by nonlinear regression and graphed semilogarithmically.

(G) Bar graph representation of the inactive compounds, fluorescein, and NSC 348718. Data represent mean with SD for triplicate samples in each case.

(for instance, 1 mM for the NCI DTP Mechanistic Sets and 10 mM for the NCI DTP Diversity Set) that would not exceed 1% dimethyl sulfoxide (DMSO) carrier solvent, the highest concentration of DMSO that did not affect the reaction or the Alpha detection (Fenteany et al., 2020).

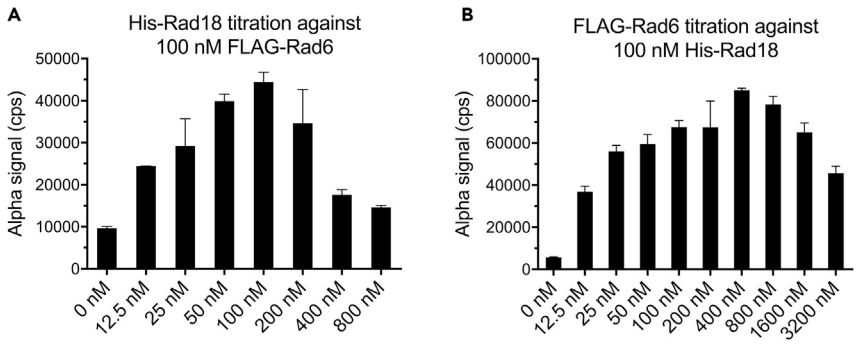

Figure 4. Development of an Alpha assay for the Rad6–Rad18 interaction

(A) Titration of His-Rad18 against FLAG-Rad6. His-Rad18 concentrations were varied as indicated, whhereas FLAG-Rad6 was held constant at 100 nM.

(B) Titration of FLAG-Rad6 against His-Rad18. FLAG-Rad6 concentrations were varied as indicated, whereas His-Rad18 was held constant at 100 nM. Data represent the mean with SD for triplicate samples in each case.

Certain xanthenes and a related acridine derivative inhibit PCNA ubiquitination

Over the course of screening compound libraries, including the NCI DTP Diversity Set VI and Mechanistic Set IV, for modulators of PCNA ubiquitination under the conditions described earlier, we identified a range of bioactive small molecules. One of the compound classes we found to strongly inhibit overall PCNA ubiquitination is composed of certain xanthenes and a related acridine derivative, identified from the NCI DTP Mechanistic Set IV and including analogs acquired thereafter (structures in Figure 2 and effects on PCNA ubiquitination in Figures 3, S2 and Table 1). Effects of the compounds in the Alpha assays for overall PCNA ubiquitination and discrete steps in the cascade were confirmed by western blot or gel-based analyses (Fenteany et al., 2019), which largely yielded parallel results (Figures S2, S3, and S4).

Activities of the compounds in secondary assays for different processes along the PCNA ubiquitination cascade

Compound dose-response experiments were carried out not only for overall PCNA ubiquitination but also for Uba1∼ubiquitin thioester formation, Rad6∼ubiquitin thioester formation, and Rad18 autoubiquitination Alpha assays (Figures 5, 6A–6F, 7 and Table 1), as previously described (Fenteany et al., 2020). Furthermore, on the basis of a Rad6–Rad18 interaction assay we developed and report here (Figure 4), we also tested the compounds in dose–response experiments for effects on the Rad6–Rad18 interaction (Figure 8), as described later.

We found that a number of the xanthen-3-ones tested—NSC 9037, NSC 80693, NSC 157411, and NSC 119888—as well as the acridine NSC 71947 inhibit formation of the Rad6∼ubiquitin thioester conjugate, whereas fluorescein, NSC 119891, and NSC 348718 do not inhibit this activity (Figures 6A–6F and Table 1). Further confirming Rad6 inhibition, the NSC 9037, NSC 80693, and NSC 157411 compounds inhibit Rad18 autoubiquitination, which depends on Rad6 activity (Figure 7 and Table 1). Some of these compounds (NSC 157411 and NSC 119888), however, appear to be less specific to Rad6 inhibition, as they inhibit Uba1∼ubiquitin thioester formation as well (Figure 5 and Table 1).

In addition to inhibiting Rad6 ubiquitin-conjugating activity, compounds binding to Rad6 can also inhibit its binding to Rad18. To investigate this possibility, we tested the compounds in a Rad6–Rad18 interaction assay and found that a subset of the xanthen-3-ones tested inhibited the association of Rad6 and Rad18 (Figures 8A–8C and Table 1). Three of the xanthen-3-ones tested—NSC 9037, NSC 80693, and NSC 157411—disrupt the Rad6–Rad18 interaction (Figures 8A–8C, S4, and Table 1). The rest of the xanthen-3-ones (NSC 119888, NSC 119891, and fluorescein), the nonketone xanthene NSC 348718, and the acridine NSC 71947 do not appreciably inhibit formation of the Rad6–Rad18 complex (Figure 8D). Fluorescein had no activity in any of the assays. These results were confirmed in a pull-down assay using Flag-Rad18 and GST-Rad6 (Figure S4). In contrast, in a heterologous assay for association of Rad6 with another E3 ubiquitin ligase, Ubr1, we found no appreciable disruption of the interaction for NSC 9037, the most potent Rad6 and Rad18 disruptor in a gel-based assay (Figure S5B), and no or very little effect of the other examined compounds as revealed by our Alpha assay (Figure S6).

Table 1. Half-maximal inhibitory concentration (IC_{50}) values by Alpha assays against PCNA ubiquitination, Uba1∼ubiquitin thioester formation, Rad6∼ubiquitin thioester formation, Rad18 autoubiquitination, Rad6–Rad18 interaction, and Mms2–Ubc13∼ubiquitin thioester formation

Compound (NSC number)	PCNA–Ub	Uba1∼Ub	Rad6∼Ub	Rad18–Ub	Rad6–Rad18	Rad6–Ubr1	Mms2–Ubc13∼Ub	IC_{50} (μM) for cell survival
9037	4.543 (SE: 0.9600; CI: 2.607–5.208)	>100	8.901 (SE: 3.050; CI: 3.945–20.97)	4.460 (SE: 1.071; CI: 2.582–7.698)	6.193 (SE: 0.8657; CI: 4.687–8.194)	>50	No inhibition on gel at 100 μM	62.23 (SE: 9.861; CI: 44.86–88.31)
80693	4.278 (SE: 0.4380; CI: 3.749–5.623)	>100	91.84 (SE: 27.7; CI: 60.67–214–)	13.22 (SE: 4.839; CI: 6.589–27.20)	14.58 (SE: 2.341; CI: 11.25–27.10)	Little inhibition by Alpha at 50 μM	No inhibition on gel at 100 μM	7.668 (SE: 4.345; CI: 0.5773–23.10)
119891	73.5 (SE: 25.26; CI: 41. 14–140.0)	>100	>100	>100	>100	Little inhibition by Alpha at 50 μM	No inhibition on gel at 100 μM	207.5 (SE: 29.38; CI: 170.0–304.2)
119888	56.5.6 (SE: 27.57; CI: 27.57–19.33–)	53.83 (SE: 19.96; CI: 26.10–139.1)	1.903 (SE: 4.087; CI: 1.205–3.094)	100	>100	No inhibition by Alpha at 50 μM	No inhibition on gel at 100 μM	75.31 (SE: 10.98; CI: 63.05–89.45)
Fluorescein	>100	>100	>100	>100	>100	Little inhibition by Alpha at 50 μM	No inhibition on gel at 100 μM	>100
157411	8.439 (SE: 2.645; CI: 4.411–16.95)	24.82 (SE: 2.556; CI: 20.18–30.57)	22.53 (SE: 3.512; CI: 16.63–40.25)	49.07 (SE: 7.231; CI: 32.27–Ind)	64.71 (SE: 19.34; CI: 40.85–360.3)	No inhibition by Alpha at 50 μM	No inhibition on gel at 100 μM	427.8 (SE: 94.90; CI: 273.9–719.9)
348718	>100	>100	>100	>100	>100	No inhibition by Alpha at 50 μM	No inhibition on gel at 100 μM	27.74 (SE: 7.404; CI: 24.56–31.35)
71947	24.89 (SE: 6.218; CI: 15.48–40.26)	>100	28.33 (SE: 7.496; CI: 16.94–47.38–)	>100	>100	Little inhibition by Alpha at 50 μM	No inhibition on gel at 100 μM	11.78 (SE: 2.910; CI: 7.199–18.27)

Also included are IC_{50} values for cell survival. All IC_{50} values, standard errors, and 95% confidence intervals listed were calculated by nonlinear regression with the GraphPad Prism 8 software. Ub = ubiquitin; SE = standard error; CI = 95% confidence interval; Ind = indeterminate.

We also tested, using a gel-based assay, the effects of the compounds on the formation of a ubiquitin conjugate with a heterologous E2 enzyme, the Mms2–Ubc13 E2 heterodimer (Figure S5A). Mms2–Ubc13 is an E2 protein complex involved in the polyubiquitination of PCNA. These results suggest that the compounds do not appear to just promiscuously inhibit all E2 enzymes.

To explore the target protein-binding properties of NSC 9037, the most specific and highly potent inhibitor of PCNA ubiquitination of the examined compounds, we used microscale thermophoresis. We revealed a K_d of 3.79 ± 2.94 μM (mean ± standard deviation [SD]) for NSC 9037 binding to Rad6 (Figure S1). At low concentrations used for the Rad6-binding study, NSC 9037 exhibited only very weak binding to Rad18, and precise K_d measurement was not possible because of the compound's fluorescence at higher concentrations in the green wavelengths at which our microscale thermophoresis instrument excites.

The compounds had varying effects on cell survival (Figure 9 and Table 1). Fluorescein had no effect on cell viability at all, whereas the other compounds ranged from moderate effects that plateaued at a not-completely inhibited state to full cytotoxicity at relatively low concentrations.

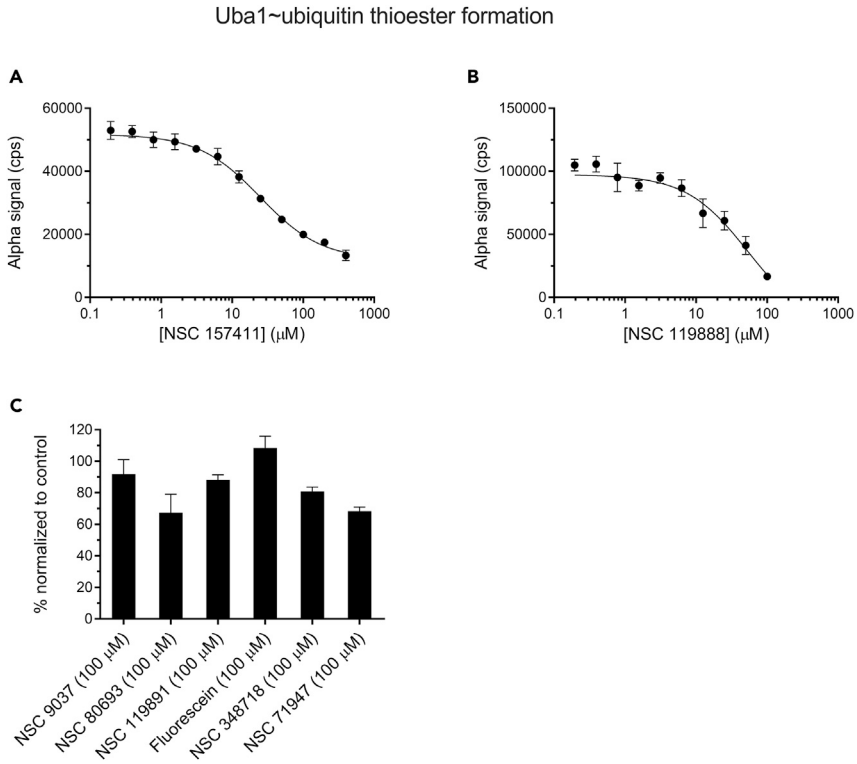

Figure 5. Dose response for Uba1~ubiquitin thioester formation in the presence of compounds by Alpha assay

(A) Dose response of NSC 157411 for Uba1~ubiquitin thioester formation.

(B) Dose response of NSC 119888 for Uba1~ubiquitin thioester formation.

Curves in (A) and (B) were fitted by nonlinear regression and graphed semilogarithmically.

(C) Bar graph representation of inactive compounds. Data represent mean with SD for triplicate samples in each case.

Identification of possible compound-binding sites

NSC 9037 was first docked to the nuclear magnetic resonance solution structure of human Rad6B (PDB ID: 2Y4W; Huang et al., 2011), followed by the other compounds. Two potential binding crevices for NSC 9037 were identified on the surface of Rad6. These locations and two representative binding orientations are shown in Figure 10A. These binding poses were then refined by performing flexible blind dockings. Furthermore, flexible blind dockings were extended to include all ten xanthene derivatives. The results obtained for the full set of compounds confirmed the location of the above-identified potential binding pockets (SN-SN+7; Figure 10B and Table 2). Polar contacts in site 1 were found to be formed most frequently with residues D12 and S60, whereas the most frequent hydrophobic contacts were formed with residues F59, P64, P68, and W96. In site two, polar contacts were provided by Y130 and Y137, whereas hydrophobic interactions were furnished most frequently by I105 and V141. The observed presumably false-positive prediction for a few of the compounds reflects the limitations of the docking method to differentiate between compounds with similar structures and polarity. Whereas geometric features are well accounted for, differences between polar functional groups in forming intermolecular interactions are roughly approximated.

DISCUSSION

In the present study, we reveal the inhibitory activity of a series of xanthenes and a related acridine derivative (NSC 71947) against different steps of the PCNA ubiquitination cascade. A subset of these compounds inhibits Rad6~ubiquitin thioester formation and disrupt the Rad6–Rad18 interaction required to ubiquitinate the K164 residue of PCNA, a key step in initiating the pathways of DNA damage bypass and tolerance. Rad6–Rad18 is the E2–E3 protein pair directly responsible for the transfer of ubiquitin from Rad6 to the K164 residue of PCNA. Inhibiting the more downstream steps in the PCNA ubiquitination cascade would be expected to yield more selective inhibition of DNA damage tolerance over other

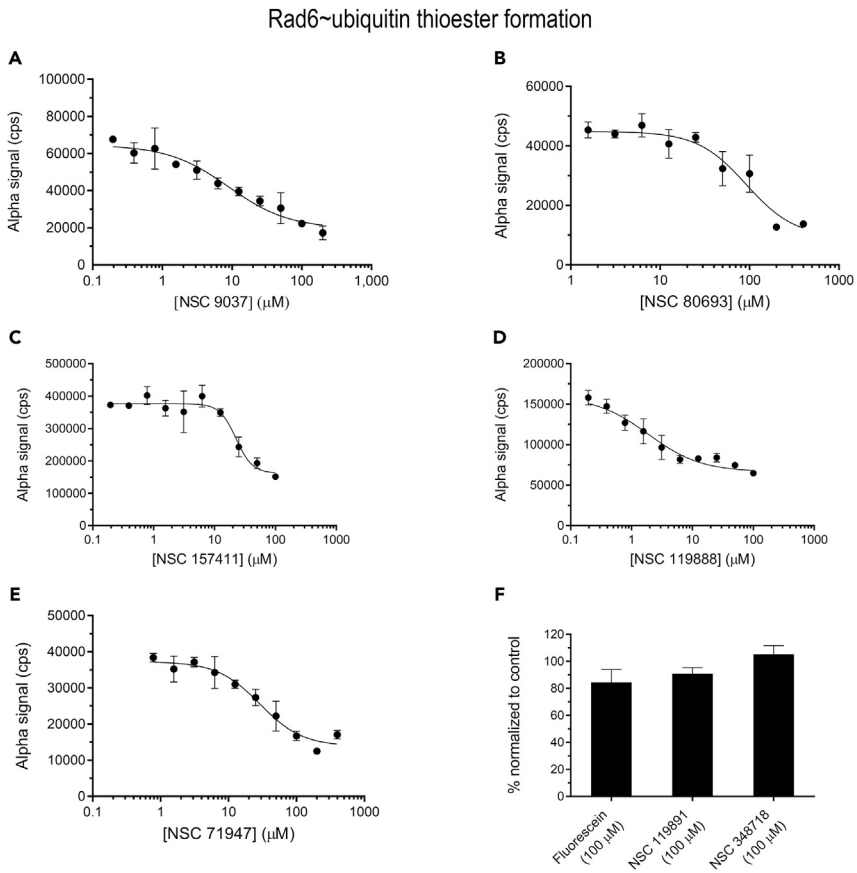

Figure 6. Effect of compounds on the formation of the Rad6∼ubiquitin thioester conjugate and the Mms2–Ubc13∼ubiquitin thioester conjugate

(A) Dose response for Rad6~ubiquitin thioester formation in the presence of NSC 9037 by Alpha assay.
(B) Dose response for Rad6~ubiquitin thioester formation in the presence of NSC 80693 by Alpha assay.
(C) Dose response for Rad6~ubiquitin thioester formation in the presence of NSC 157411 by Alpha assay.
(D) Dose response for Rad6~ubiquitin thioester formation in the presence of NSC 119888 by Alpha assay.
(E) Dose response for Rad6~ubiquitin thioester formation in the presence of NSC 71947 by Alpha assay.
The graphs in (A)–(E) were plotted semilogarithmically.
(F) Bar graph representation of inactive compounds. Data represent mean with SD for triplicate samples in each case.

ubiquitin- or UBL-based pathways. The inhibitory compounds we describe here are related to other xanthene dyes such as rhodamine and eosin, as well as, of course, fluorescein, which we found to be inactive in all of our assays. The compounds inhibit Rad6∼ubiquitin thioester formation and some also disrupt the interaction of Rad6 with Rad18, the latter an RING class E3 protein ligase with a narrow range of target substrates—in particular, PCNA on its K164 residue.

Of the components of the PCNA ubiquitination cascade, Uba1, the ubiquitin-activating enzyme responsible for the first step in virtually all ubiquitination pathways in the cell, is probably the most "druggable" of the proteins in the pathway, both as direct and indirect target, based on our (Fenteany et al., 2019, 2020) and others' (Sekizawa et al., 2002; Tsukamoto et al., 2005; Yang et al., 2007; Lu et al., 2010; Xu et al., 2010b; Hong and Luesch, 2012; Ungermannova et al., 2012a, 2012b, 2013; Yamanokuchi et al., 2012; An and Statsyuk, 2013, 2015; Hyer et al., 2018; Hann et al., 2019) empirical experience, as well as structural and docking studies, with at least four putative general compound-binding hot spot pockets, as computationally predicted (Lv et al., 2018). There are a fair number of different Uba1 inhibitors (Fenteany et al., 2019, 2020; Sekizawa et al., 2002; Tsukamoto et al., 2005; Yang et al., 2007; Lu et al., 2010; Xu et al., 2010b; Hong and Luesch, 2012; Ungermannova et al., 2012a, 2012b, 2013; Yamanokuchi et al., 2012; An and Statsyuk, 2013, 2015; Hyer et al., 2018; Hann et al., 2019), but only one known class of

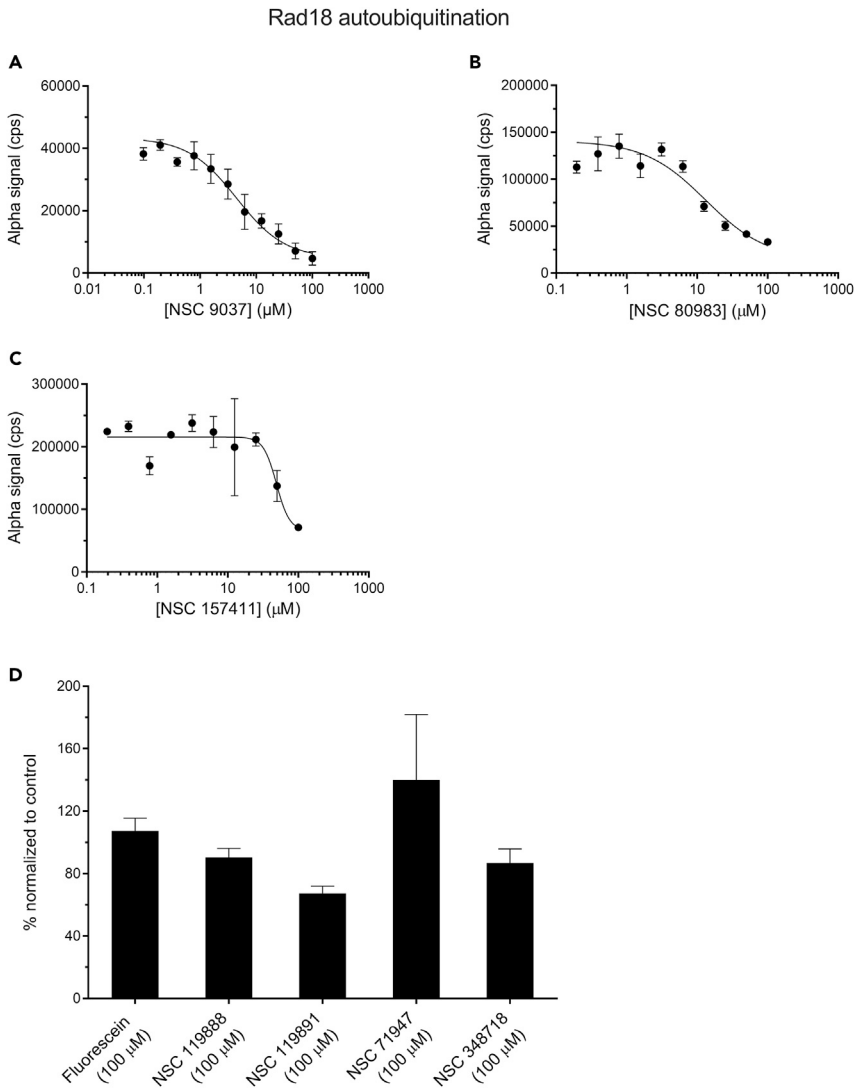

Figure 7. Dose response for autoubiquitination of Rad18 in the presence of compounds by Alpha assay

(A) Dose response of NSC 9037 for autoubiquitination of Rad18.

(B) Dose response of NSC 80983 for autoubiquitination of Rad18.

(C) Dose response of NSC 157411 for autoubiquitination of Rad18.

Semilogarithmic plots are graphed in (A)–(C).

(D) Bar graph representation of inactive compounds. Data represent mean with SD for triplicate samples in each case.

inhibitors of Rad6~ubiquitin thioester conjugate formation (Sanders et al., 2013, 2017; Haynes et al., 2015a, 2015b, 2020; Saadat et al., 2018). No compound has yet been reported that interferes with the association of Rad6 with Rad18.

Preliminary structure-activity relationships suggest that certain groups and their placement are important for activity. The compounds exhibit different selectivities in different assays (Figures 3, 5, 6, 7, 8, and 9, and Table 1), with only a subset of the xanthen-3-ones, but not the other xanthenes or the acridine derivative, inhibiting the Rad6–Rad18 interaction (Figure 8). Fluorescein itself, the ortho-substituted constitutional isomer of NSC 119891 and NSC 119888, had no activity in any of the assays. The meta- and para-substituted isomers (NSC 119888 and NSC 119891, respectively) were biologically active in a number of assays; this demonstrates that placement of the carboxylic acid on these isomeric xanthen-3-ones is a critical determinant of activity. Fluorescein can also cyclize to a phthalein product because of the ortho placement of the carboxylic acid on the phenyl ring. In addition, NSC 157411, which differs from

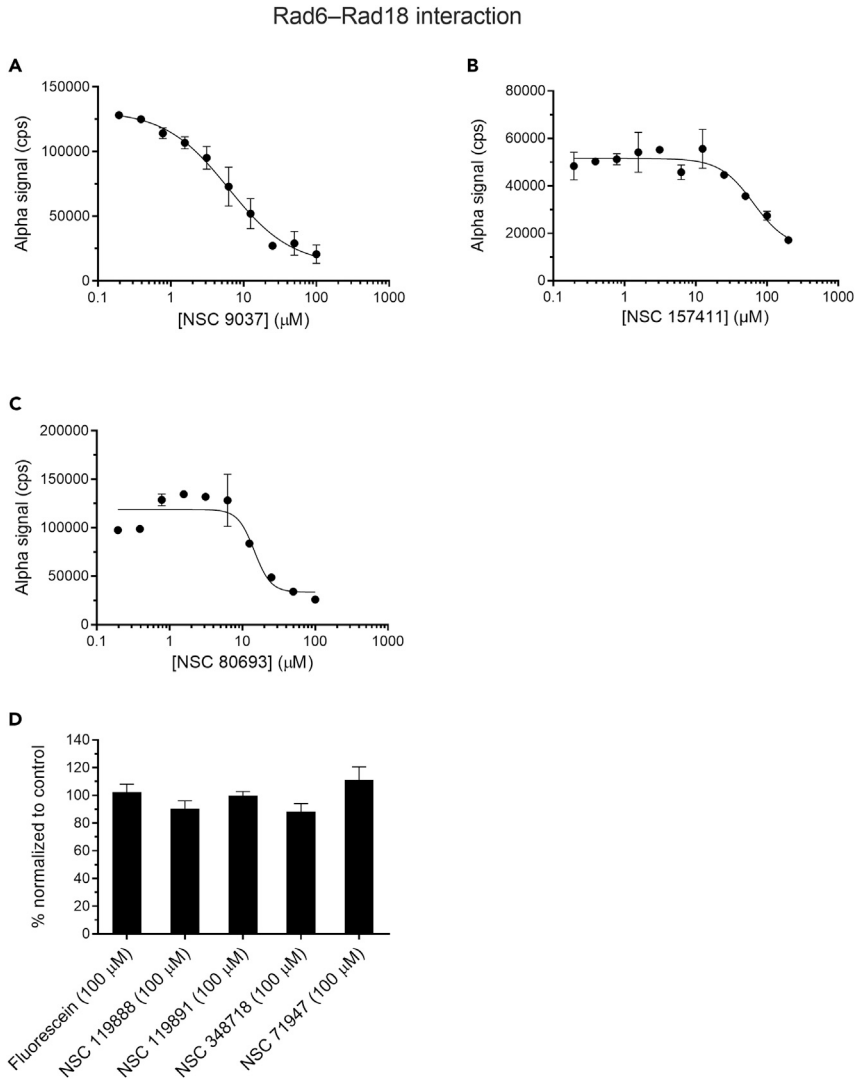

Figure 8. Dose–response for the Rad6–Rad18 interaction in the presence of compounds by Alpha assay

(A) Dose response of NSC 9037 for Rad6–Rad18 interaction.

(B) Dose response of NSC 157411 for Rad6–Rad18 interaction.

(C) Dose response of NSC 80693 for Rad6–Rad18 interaction.

Semilogarithmic plots are graphed in (A)–(C).

(D) Bar graph representation of inactive compounds. Data represent mean with SD for triplicate samples in each case.

fluorescein in having a cyclohexene in place of the phenyl ring, also exhibits biological activity. Furthermore, the selective activities of the bioactive compounds against different proteins argue that these molecules are not just pan-assay interference compounds, whose effects could be ascribed to, for instance, simple colloidal aggregation. However, several of the molecules did tend to aggregate at higher concentration over time.

NSC 9037 binds Rad6 with a K_d of 3.79 μM by microscale thermophoresis (Figure S1). NSC 9037 also has the highest affinity for Rad6 of all the compounds in blind dockings. The computational results predict two sites of binding for the compounds, one or two of which all of the bioactive compounds appear to bind (Table 2). These two putative compound-binding sites are not located near the catalytic cysteine residue involved in thioester formation with ubiquitin (C88 in human Rad6B), suggesting that, if the predictions are correct, the inhibition of Rad6~ubiquitin thioester formation is exerted through an allosteric mechanism involving large conformational changes.

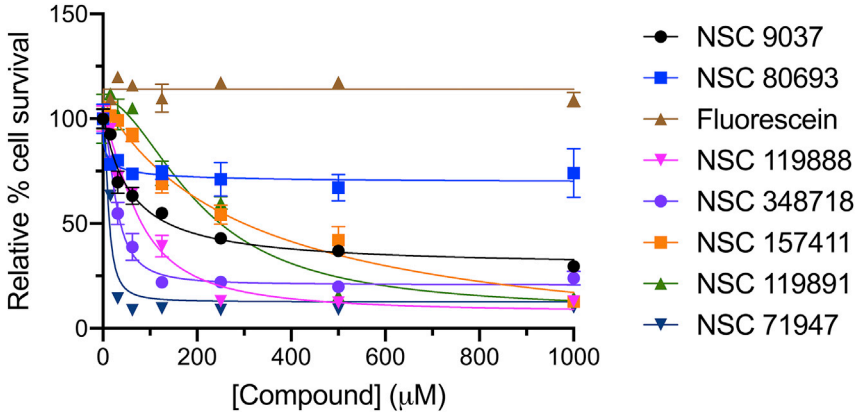

Figure 9. Effect of compounds on the viability of HeLa cells

Data represent mean with SD for triplicate samples in each case. Semilogarithmic plots are graphed.

With regard to the Rad6–Rad18 interaction, comparing these putative compound-binding sites to the C-terminal location of the Rad6-binding domain (Rad6BD) on Rad18, one of the major interfaces of interaction between Rad6 and Rad18 (Bailly et al., 1997; Hibbert et al., 2011; Notenboom et al., 2007), as shown in an X-ray co-crystal structure [(PDB ID: 2YBF) (Hibbert et al., 2011)], we observed that the two putative binding sites for the compounds lie on either side of the Rad6BD-binding site on Rad6. The Rad6BD also overlaps with the noncovalent ubiquitin-binding of Rad6 (Hibbert et al., 2011). It is easy to envision that compound binding can induce local conformational changes and, subsequently, changes in the local distribution of partial atomic charges that lower affinity of Rad6 with the Rad6BD. The RING domain located near the N-terminus of Rad18 also contributes to Rad6–Rad18 interactions (Huang et al., 2011; Masuda et al., 2012; Notenboom et al., 2007). This protein domain–protein domain interaction site is also on the same face of the protein as the putative binding sites for the compounds, and this interaction may also be affected by compound binding.

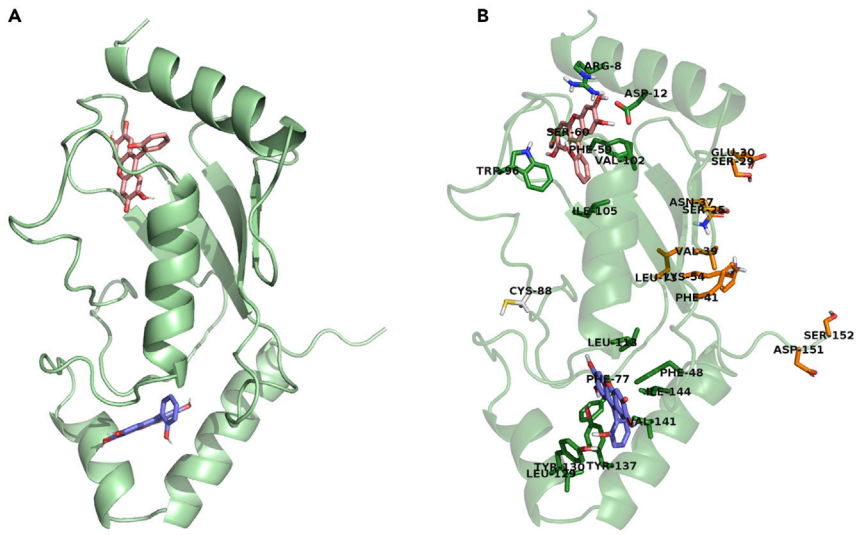

Figure 10. Computational docking of NSC 9037 to Rad6B

(A) Potential binding sites and poses of NSC 9037 on Rad6 identified by initial blind dockings of flexible compounds to rigid protein surfaces.

(B) Refined binding poses of NSC 9037 on Rad6 are shown in pink and purple; amino acid residues in contact with NSC 9037 in green; those in close proximity to the putative compound-binding sites and involved in Rad18's Rad6BD–Rad6 interaction in orange; and the catalytic cysteine residue (C88) on Rad6 in white.

Table 2. *In silico* binding affinities and amino acid side chains of human Rad6B in contact with the tested ligands, obtained from refined docking of flexible compounds to flexible protein surfaces

Compound	Grid (site)	K_i (nM)	Polar contacts	Hydrophobic contacts
NSC 9037	1	0.1	R^{8}, D^{12}, S^{60}	L^{9}, I^{57}, F^{59}, P^{64}, P^{68}, W^{96}, V^{102}, I^{105}
	2	90.2	H^{78}, Y^{130}, Y^{137}	P^{47}, F^{48}, P^{79}, L^{113}, P^{116}, V^{141}
NSC 80693	1	<0.1	R^{8}, D^{12}, S^{60}	L^{9}, F^{59}, P^{64}, P^{68}, I^{105}
	2	24.5	Q^{125}, Y^{130}	F^{77}, V^{81}, I^{105}, L^{129}, Y^{137}, V^{141}
NSC 119891	1	7.8	—	F^{59}, P^{64}, P^{68}, W^{96}, I^{105}
	2	11.4	H^{78}, Y^{130}, Y^{137}	P^{47}, F^{48}, P^{79}, V^{141}
NSC 119888	1	0.7	S^{60}	F^{59}, P^{68}, W^{96}, I^{105}
	2	0.9	Y^{130}, Y^{137}	P^{47}, F^{77}, P^{79}, L^{113}, P^{116}, L^{129} V^{141}
Fluorescein	1	2.0	D^{12}, S^{60}, D^{101}	F^{59}, P^{68}, W^{96}, V^{102}, I^{105}
	2	26.2	Y^{130}, R^{140}	F^{77}, L^{129} V^{141}
NSC 157411	1	1.1	R^{8}, D^{12}, S^{60}	F^{59}, P^{64}, P^{68}, W^{96}, I^{105}
	2	0.9	Y^{130}, Y^{137}	P^{47}, F^{48}, F^{77}, P^{79}, P^{116}, V^{141}
NSC 348718	1	1.7	D^{12}, S^{60}, D^{101}	R^{8}, F^{59}, P^{64}, P^{68}, W^{96}, I^{105}
	2	19.3	—	P^{47}, F^{48}, P^{79}, P^{116}, Y^{130}, Y^{137}, V^{141}
NSC 71947	1	66.4	S^{60}	R^{8}, F^{59}, P^{64}, P^{68}, V^{102}, I^{105}
	2	92.2	Y^{130}	P^{79}, L^{113}, P^{116}, Y^{137}, V^{141}

All of the compounds that disrupt the Rad6–Rad18 interaction are xanthen-3-ones, although not all of the xanthen-3-ones do, so this core structure may be a part of, but not the only determinant of, activity against interaction between Rad6 and Rad18. Similarly, all of the compounds that affect Rad6~ubiquitin thioester formation are also xanthen-3-ones. A smaller subset of xanthen-3-ones affect both Rad6~ubiquitin thioester formation and the Rad6–Rad18 interaction. These compounds would be expected to induce considerable conformational changes, as the active-site cysteine (C88 in human Rad6B) and the regions of interaction with Rad18 are on opposite faces of Rad6.

It is interesting to note that although the Rad6–Rad18 complex has long been considered highly stable (Bailly et al., 1994), these compounds disrupt the interaction between preformed Rad6–Rad18 complexes. The mechanism could either be a direct dissociation on binding an exposed site important for the Rad6–Rad18 interaction or could involve binding the fraction of dissociated protein and preventing association, driving the equilibrium toward a fully dissociated state through mass action.

In summary, we report here a series of xanthenes, most of which inhibit PCNA ubiquitination, with a subset of them inhibiting Rad6~ubiquitin thioester formation and disrupting the interaction of Rad6 with Rad18 (which are only active for ubiquitination of relevant substrates in the form of a complex). These compounds may serve as a starting point for medicinal chemistry efforts to improve activity and for further investigating the molecular basis and therapeutic control of Rad6~ubiquitin thioester formation and Rad6–Rad18 interactions.

Limitations of the study

The main value of our study is that the series of xanthenes we tested represent first-in-class probes of Rad6 function and the association of Rad6 and Rad18. Here we focus on *in vitro* approaches apart from the evaluation of the effects of the compounds on cell survival; however, we are aware that the potency and efficacy of the compounds should be explored with more extensive cellular experiments. These could include cellular PCNA ubiquitylation assays, mutagenesis, DNA fiber, and Comet assays as well, to explore the effect of these compounds on replication and DNA damage bypass. Our most promising compounds such as NSC 9037 exhibit dual activity, as they inhibit Rad6-Ubiquitin-thioester formation as well as Rad6-Rad18 interaction. We propose that inhibiting these activities is the underlying cause of inhibiting PCNA ubiquitylation. The question arises whether these compounds can inhibit other E2s or interactions of Rad6 with its other E3 partners such as Ubr1, which would result in inhibiting other cellular ubiquitination events in

addition to PCNA ubiquitination. Although we found that our tested compounds do not inhibit Mms2-Ubc13 E2 and the interaction of Rad6 with Ubr1 E3, we cannot formally rule out that even our most promising compounds can interfere with other Rad6-mediated cellular events such as histone ubiquitylation. Clearly, other analogues of xanthenes with particular focus on the analogues of NSC9037 should be explored via structural and mutagenesis studies to determine their Rad6-binding site and find the most potent and specific inhibitor of Rad6-Rad18 interaction, followed by testing their effect on various cellular ubiquitination events including PCNA and histone ubiquitination.

STAR★METHODS

Detailed methods are provided in the online version of this paper and include the following:

- KEY RESOURCES TABLE
- RESOURCE AVAILABILITY
  - Lead contact
  - Materials availability
  - Data and code availability
- EXPERIMENTAL MODEL AND SUBJECT DETAILS
  - Microbes
  - Cell lines
- METHOD DETAILS
  - Protein preparation
  - Generation of GFP-Rad6 and GFP-Rad18 fusion constructs
  - Alpha assays
  - PCNA ubiquitination
  - Uba1~ubiquitin thioester formation
  - Rad6~ubiquitin thioester formation
  - Rad18 autoubiquitination
  - Rad6–Rad18 interaction
  - Mms2–Ubc13~ubiquitin thioester formation
  - Microscale thermophoresis
  - Rad6–Ubr1 pull-down
  - Rad6–Ubr1 interaction alpha assay
  - Cell culture
  - Cell survival
  - Computational docking of compounds to Rad6
- QUANTIFICATION AND STATISTICAL ANALYSIS

SUPPLEMENTAL INFORMATION

Supplemental information can be found online at https://doi.org/10.1016/j.isci.2022.104053.

ACKNOWLEDGMENTS

We wish to acknowledge Tamás Martinek for sharing his expertise, as well as Katalin Kovacs, Katalin Kontár, and Éva Hunyadi-Gulyas for their technical assistance and Gabriella Tick for proofreading the manuscript. We thank the US National Cancer Institute's Developmental Therapeutics Program for providing chemical libraries and individual compounds. This work was supported by the National Research, Development and Innovation Office (GINOP-2.3.2–15-2016–00024 and GINOP-2.2.1-15-2017-00072). This project has also received funding from the European Union's Horizon 2020 Research And Innovation Program under grant agreement No. 739593.

AUTHOR CONTRIBUTIONS

GF and LH conceived and directed the project. GS did most of the experiments, PG performed microscale thermophoresis, AB conducted computational studies, and EK made the plasmid constructs. GF, GS, EW, and AB analyzed the data. GF wrote the bulk of the manuscript. All authors read and approved the final manuscript.

DECLARATION OF INTERESTS

The authors declare no competing interests.

Received: June 15, 2021
Revised: December 13, 2021
Accepted: March 8, 2022
Published: April 15, 2022

REFERENCES

Altieri, A.S., and Kelman, Z. (2018). DNA sliding clamps as therapeutic targets. Front. Mol. Biosci. *5*, 87. https://doi.org/10.3389/fmolb.2018.00087.

An, H., and Statsyuk, A.V. (2015). An inhibitor of ubiquitin conjugation and aggresome formation. Chem. Sci. *6*, 5235–5245. https://doi.org/10.1039/c5sc01351h.

An, H., and Statsyuk, A.V. (2013). Development of activity-based probes for ubiquitin and ubiquitin-like protein signaling pathways. J. Am. Chem. Soc. *135*, 16948–16962. https://doi.org/10.1021/ja4099643.

Bailly, V., Lamb, J., Sung, P., Prakash, S., and Prakash, L. (1994). Specific complex formation between yeast RAD6 and RAD18 proteins: a potential mechanism for targeting RAD6 ubiquitin-conjugating activity to DNA damage sites. Genes Dev. *8*, 811–820. https://doi.org/10.1101/gad.8.7.811.

Bailly, V., Prakash, S., and Prakash, L. (1997). Domains required for dimerization of yeast RAD6 ubiquitin-conjugating enzyme and RAD18 DNA binding protein. Mol. Cell. Biol. *17*, 4536–4543. https://doi.org/10.1128/MCB.17.8.4536.

Branzei, D., and Szakal, B. (2017). Building up and breaking down: mechanisms controlling recombination during replication. Crit. Rev. Biochem. Mol. Biol. *52*, 381–394. https://doi.org/10.1080/10409238.2017.1304355.

Branzei, D., and Szakal, B. (2016). DNA damage tolerance by recombination: molecular pathways and DNA structures. DNA Repair (Amst.) *44*, 68–75. https://doi.org/10.1016/J.DNAREP.2016.05.008.

Cardano, M., Tribioli, C., and Prosperi, E. (2020). Targeting proliferating cell nuclear antigen (PCNA) as an effective strategy to inhibit tumor cell proliferation. Curr. Cancer Drug Targets *20*, 240–252. https://doi.org/10.2174/1568009620666200115162814.

Choe, K.N., and Moldovan, G.L. (2017). Forging ahead through darkness: PCNA, still the principal conductor at the replication fork. Mol. Cell *65*, 380–392. https://doi.org/10.1016/j.molcel.2016.12.020.

Dieckman, L.M., Freudenthal, B.D., and Washington, M.T. (2012). PCNA structure and function: insights from structures of PCNA complexes and post-translationally modified PCNA. Subcell. Biochem. *62*, 281–299. https://doi.org/10.1007/978-94-007-4572-8_15.

Fan, L., Bi, T., Wang, L., and Xiao, W. (2020). DNA-damage tolerance through PCNA ubiquitination and sumoylation. Biochem. J. *477*, 2655–2677. https://doi.org/10.1042/BCJ20190579.

Fenteany, G., Gaur, P., Hegedűs, L., Dudás, K., Kiss, E., Wéber, E., Hackler, L., Martinek, T., Puskás, L.G., and Haracska, L. (2019). Multilevel structure–activity profiling reveals multiple green tea compound families that each modulate ubiquitin-activating enzyme and ubiquitination by a distinct mechanism. Sci. Rep. *9*, 12801. https://doi.org/10.1038/s41598-019-48888-6.

Fenteany, G., Gaur, P., Sharma, G., Pintér, L., Kiss, E., and Haracska, L. (2020). Robust high-throughput assays to assess discrete steps in ubiquitination and related cascades. BMC Mol. Cell Biol. *21*, 21. https://doi.org/10.1186/s12860-020-00262-5.

Finkelstein, J., Antony, E., Hingorani, M.M., and O'Donnell, M. (2003). Overproduction and analysis of eukaryotic multiprotein complexes in escherichia coli using a dual-vector strategy. Anal. Biochem. *319*, 78–87. https://doi.org/10.1016/S0003-2697(03)00273-2.

Gallo, D., and Brown, G.W. (2019). Post-replication repair: Rad5/HLTF regulation, activity on undamaged templates, and relationship to cancer. Crit. Rev. Biochem. Mol. Biol. *54*, 301–332. https://doi.org/10.1080/10409238.2019.1651817.

Ghahsare, A.G., Nazifi, Z.S., and Nazifi, S.M.R. (2019). Structure-bioactivity relationship study of xanthene derivatives: a brief review. Curr. Org. Synth. *16*, 1071–1077. https://doi.org/10.2174/1570179416666191017094908.

Hann, Z.S., Ji, C., Olsen, S.K., Lu, X., Lux, M.C., Tan, D.S., and Lima, C.D. (2019). Structural basis for adenylation and thioester bond formation in the ubiquitin E1. Proc. Natl. Acad. Sci. U S A *116*, 15475–15484. https://doi.org/10.1073/pnas.1905488116.

Haracska, L., Unk, I., Prakash, L., and Prakash, S. (2006). Ubiquitylation of yeast proliferating cell nuclear antigen and its implications for translesion DNA synthesis. Proc. Natl. Acad. Sci. U S A *103*, 6477–6482. https://doi.org/10.1073/pnas.0510924103.

Haynes, B., Gajan, A., Nangia-Makker, P., and Shekhar, M.P. (2020). RAD6B is a major mediator of triple negative breast cancer cisplatin resistance: regulation of translesion synthesis/Fanconi anemia crosstalk and BRCA1 independence. Biochim. Biophys. Acta Mol. Basis Dis. *1866*, 165561. https://doi.org/10.1016/j.bbadis.2019.165561.

Haynes, B., Saadat, N., Myung, B., and Shekhar, M.P.V. (2015a). Crosstalk between translesion synthesis, Fanconi anemia network, and homologous recombination repair pathways in interstrand DNA crosslink repair and development of chemoresistance. Mutat. Res. *763*, 258–266. https://doi.org/10.1016/j.mrrev.2014.11.005.

Haynes, B., Zhang, Y., Liu, F., Li, J., Petit, S., Kothayer, H., Bao, X., Westwell, A.D., Mao, G., and Shekhar, M.P.V. (2015b). Gold nanoparticle conjugated Rad6 inhibitor induces cell death in triple negative breast cancer cells by inducing mitochondrial dysfunction and PARP-1 hyperactivation: synthesis and characterization. Nanomedicine *12*, 745–757. https://doi.org/10.1016/j.nano.2015.10.010.

Hibbert, R.G., Huang, A., Boelens, R., and Sixma, T.K. (2011). E3 ligase Rad18 promotes monoubiquitination rather than ubiquitin chain formation by E2 enzyme Rad6. Proc. Natl. Acad. Sci. U S A *108*, 5590–5595. https://doi.org/10.1073/pnas.1017516108.

Hong, J., and Luesch, H. (2012). Largazole: from discovery to broad-spectrum therapy. Nat. Prod. Rep. *29*, 449–456. https://doi.org/10.1039/c2np00066k.

Horsfall, A.J., Abell, A.D., and Bruning, J.B. (2020). Targeting PCNA with Peptide Mimetics for Therapeutic Purposes, ChemBioChem (Wiley-VCH Verlag). https://doi.org/10.1002/cbic.201900275.

Huang, A., Hibbert, R.G., De Jong, R.N., Das, D., Sixma, T.K., and Boelens, R. (2011). Symmetry and asymmetry of the RING-RING dimer of Rad18. J. Mol. Biol. *410*, 424–435. https://doi.org/10.1016/j.jmb.2011.04.051.

Hyer, M.L., Milhollen, M.A., Ciavarri, J., Fleming, P., Traore, T., Sappal, D., Huck, J., Shi, J., Gavin, J., Brownell, J., et al. (2018). A small-molecule inhibitor of the ubiquitin activating enzyme for cancer treatment. Nat. Med. *24*, 186–193. https://doi.org/10.1038/nm.4474.

Jiang, Q., Zhang, W., Liu, C., Lin, Y., Wu, Q., and Dai, J. (2019). Dissecting PCNA function with a systematically designed mutation library in yeast. J. Genet. Genomics *46*, 301–313. https://doi.org/10.1101/352286.

Juhasz, S., Balogh, D., Hajdu, I., Burkovics, P., Villamil, M.A., Zhuang, Z., and Haracska, L. (2012). Characterization of human Spartan/C1orf124, an ubiquitin-PCNA interacting regulator of DNA damage tolerance. Nucleic Acids Res *40*, 10795–10808. https://doi.org/10.1093/nar/gks850.

Kanao, R., and Masutani, C. (2017). Regulation of DNA damage tolerance in mammalian cells by post-translational modifications of PCNA. Mutat. Res. *803–805*, 82–88. https://doi.org/10.1016/j.mrfmmm.2017.06.004.

Knobel, P.A., and Marti, T.M. (2011). Translesion DNA synthesis in the context of cancer research. Cancer Cell Int. *11*, 39. https://doi.org/10.1186/1475-2867-11-39.

Leung, W., Baxley, R., Moldovan, G.-L., and Bielinsky, A.-K. (2018). Mechanisms of DNA damage tolerance: post-translational regulation of PCNA. Genes (Basel) *10*, 10. https://doi.org/10.3390/genes10010010.

Lu, X., Olsen, S.K., Capili, A.D., Cisar, J.S., Lima, C.D., and Tan, D.S. (2010). Designed semisynthetic protein inhibitors of Ub/Ubl E1 activating enzymes. J. Am. Chem. Soc. *132*, 1748–1749. https://doi.org/10.1021/ja9088549.

Lv, Z., Williams, K.M., Yuan, L., Atkison, J.H., and Olsen, S.K. (2018). Crystal structure of a human ubiquitin E1–ubiquitin complex reveals conserved functional elements essential for activity. J. Biol. Chem. *293*, 18337–18352. https://doi.org/10.1074/jbc.RA118.003975.

Maia, M., Resende, D.I.S.P., Durães, F., Pinto, M.M.M., and Sousa, E. (2021). Xanthenes in medicinal chemistry - synthetic strategies and biological activities. Eur. J. Med. Chem. *210*, 113085. https://doi.org/10.1016/j.ejmech.2020.113085.

Masuda, Y., Suzuki, M., Kawai, H., Suzuki, F., and Kamiya, K. (2012). Asymmetric nature of two subunits of RAD18, a RING-type ubiquitin ligase E3, in the human RAD6A-RAD18 ternary complex. Nucleic Acid Res. *40*, 1065–1076. https://doi.org/10.1093/nar/gkr805.

Miyase, S., Tateishi, S., Watanabe, K., Tomita, K., Suzuki, K., Inoue, H., and Yamaizumi, M. (2005). Differential regulation of Rad18 through Rad6-dependent mono- and polyubiquitination. J. Biol. Chem. *280*, 515–524. https://doi.org/10.1074/jbc.M409219200.

Notenboom, V., Hibbert, R.G., van Rossum-Fikkert, S.E., Olsen, J.V., Mann, M., and Sixma, T.K. (2007). Functional characterization of Rad18 domains for Rad6, ubiquitin, DNA binding and PCNA modification. Nucleic Acids Res. *35*, 5819–5830. https://doi.org/10.1093/nar/gkm615.

Park, J.M., Yang, S.W., Yu, K.R., Ka, S.H., Lee, S.W., Seol, J.H., Jeon, Y.J., and Chung, C.H. (2014). Modification of PCNA by ISG15 plays a crucial role in termination of error-prone translesion DNA synthesis. Mol. Cell *54*, 626–638. https://doi.org/10.1016/j.molcel.2014.03.031.

Povlsen, L.K., Beli, P., Wagner, S.A., Poulsen, S.L., Sylvestersen, K.B., Poulsen, J.W., Nielsen, M.L., Bekker-Jensen, S., Mailand, N., and Choudhary, C. (2012). Systems-wide analysis of ubiquitylation dynamics reveals a key role for PAF15 ubiquitylation in DNA-damage bypass. Nat. Cell Biol. *14*, 1089–1098. https://doi.org/10.1038/ncb2579.

Prado, F. (2018). Homologous recombination: to fork and beyond. Genes *9*. https://doi.org/10.3390/GENES9120603.

Ripley, B.M., Gildenberg, M.S., and Todd Washington, M. (2020). Control of DNA damage bypass by ubiquitylation of PCNA. Genes *11*, 138. https://doi.org/10.3390/genes11020138.

Saadat, N., Liu, F., Haynes, B., Nangia-Makker, P., Bao, X., Li, J., Polin, L.A., Gupta, S., Mao, G., and Shekhar, M.P. (2018). Nano-delivery of RAD6/translesion synthesis inhibitor SMI#9 for triple-negative breast cancer therapy. Mol. Cancer Ther. *17*, 2586–2597. https://doi.org/10.1158/1535-7163.MCT-18-0364.

Saha, P., Mandal, T., Talukdar, A.D., Kumar, D., Kumar, S., Tripathi, P.P., Wang, Q.E., and Srivastava, A.K. (2020). DNA polymerase eta: a potential pharmacological target for cancer therapy. J. Cell Physiol. *236*, 4106–4120. https://doi.org/10.1002/jcp.30155.

Sanders, M.A., Brahemi, G., Nangia-Makker, P., Balan, V., Morelli, M., Kothayer, H., Westwell, A.D., and Shekhar, M.P.V. (2013). Novel inhibitors of Rad6 ubiquitin conjugating enzyme: design, synthesis, identification, and functional characterization. Mol. Cancer Ther. *12*, 373–383. https://doi.org/10.1158/1535-7163.MCT-12-0793.

Sanders, M.A., Haynes, B., Nangia-Makker, P., Polin, L.A., and Shekhar, M.P. (2017). Pharmacological targeting of RAD6 enzyme-mediated translesion synthesis overcomes resistance to platinum-based drugs. J. Biol. Chem. *292*, 10347–10363. https://doi.org/10.1074/jbc.M117.792192.

Sekizawa, R., Ikeno, S., Nakamura, H., Naganawa, H., Matsui, S., Iinuma, H., and Takeuchi, T. (2002). Panepophenanthrin, from a mushroom strain, a novel inhibitor of the ubiquitin-activating enzyme. J. Nat. Prod. *65*, 1491–1493. https://doi.org/10.1021/np020098q.

Slade, D. (2018). Maneuvers on PCNA rings during DNA replication and repair. Genes (Basel) *9*, 416. https://doi.org/10.3390/genes9080416.

Tonzi, P., and Huang, T.T. (2019). Role of Y-family translesion DNA polymerases in replication stress: implications for new cancer therapeutic targets. DNA Repair (Amst.) *78*, 20–26. https://doi.org/10.1016/j.dnarep.2019.03.016.

Treco, D.A., and Winston, F. (2008). Growth and manipulation of yeast. Curr. Protoc. Mol. Biol. *82*. https://doi.org/10.1002/0471142727.mb1302s82.

Tsukamoto, S., Hirota, H., Imachi, M., Fujimuro, M., Onuki, H., Ohta, T., and Yokosawa, H. (2005). Himeic acid A: a new ubiquitin-activating enzyme inhibitor isolated from a marine-derived fungus, Aspergillus sp. Bioorg. Med. Chem. Lett. *15*, 191–194. https://doi.org/10.1016/j.bmcl.2004.10.012.

Ungermannova, D., Lee, J., Zhang, G., Dallmann, H.G., McHenry, C.S., and Liu, X. (2013). High-throughput screening AlphaScreen assay for identification of small-molecule inhibitors of ubiquitin E3 ligase SCF Skp2-Cks1. J. Biomol. Screen. *18*, 910–920. https://doi.org/10.1177/1087057113485789.

Ungermannova, D., Parker, S.J., Nasveschuk, C.G., Chapnick, D.A., Phillips, A.J., Kuchta, R.D., and Liu, X. (2012a). Identification and mechanistic studies of a novel ubiquitin E1 inhibitor. J. Biomol. Screen. *17*, 421–434. https://doi.org/10.1177/1087057111433843.

Ungermannova, D., Parker, S.J., Nasveschuk, C.G., Wang, W., Quade, B., Zhang, G., Kuchta, R.D., Phillips, A.J., and Liu, X. (2012b). Largazole and its derivatives selectively inhibit ubiquitin activating enzyme (E1). PLoS One *7*, e29208. https://doi.org/10.1371/journal.pone.0029208.

Unk, I., Hajdú, I., Fátyol, K., Hurwitz, J., Yoon, J.-H., Prakash, L., Prakash, S., and Haracska, L. (2008). Human HLTF functions as a ubiquitin ligase for proliferating cell nuclear antigen polyubiquitination. Proc. Natl. Acad. Sci. U S A *105*, 3768–3773. https://doi.org/10.1073/pnas.0800563105.

Vaisman, A., and Woodgate, R. (2017). Translesion DNA polymerases in eukaryotes: what makes them tick? Crit. Rev. Biochem. Mol. Biol. *52*, 274–303. https://doi.org/10.1080/10409238.2017.1291576.

Wilkinson, N.A., Mnuskin, K.S., Ashton, N.W., and Woodgate, R. (2020). Ubiquitin and ubiquitin-like proteins are essential regulators of DNA damage bypass. Cancers *12*, 2848. https://doi.org/10.3390/cancers12102848.

Xu, G., Paige, J.S., and Jaffrey, S.R. (2010a). Global analysis of lysine ubiquitination by ubiquitin remnant immunoaffinity profiling. Nat. Biotech. *28*, 868–873. https://doi.org/10.1038/nbt.1654.

Xu, G.W., Ali, M., Wood, T.E., Wong, D., Maclean, N., Wang, X., Gronda, M., Skrtic, M., Li, X., Hurren, R., et al. (2010b). The ubiquitin-activating enzyme E1 as a therapeutic target for the treatment of leukemia and multiple myeloma. Blood *115*, 2251–2259. https://doi.org/10.1182/blood-2009-07-231191.

Yamanokuchi, R., Imada, K., Miyazaki, M., Kato, H., Watanabe, T., Fujimuro, M., Saeki, Y., Yoshinaga, S., Terasawa, H., Iwasaki, N., et al. (2012). Hyrtioreticulins A–E, indole alkaloids inhibiting the ubiquitin-activating enzyme, from the marine sponge Hyrtios reticulatus. Bioorg. Med. Chem. *20*, 4437–4442. https://doi.org/10.1016/j.bmc.2012.05.044.

Yang, W., and Gao, Y. (2018). Translesion and repair DNA polymerases: diverse structure and mechanism. Annu. Rev. Biochem. *87*, 239–261. https://doi.org/10.1146/annurev-biochem-062917-012405.

Yang, Y., Kitagaki, J., Dai, R.-M., Tsai, Y.C., Lorick, K.L., Ludwig, R.L., Pierre, S.A., Jensen, J.P., Davydov, I.V., Oberoi, P., et al. (2007). Inhibitors of ubiquitin-activating enzyme (E1), a new class of potential cancer therapeutics. Cancer Res. *67*, 9472–9481. https://doi.org/10.1158/0008-5472.CAN-07-0568.

Zafar, M.K., and Eoff, R.L. (2017). Translesion DNA synthesis in cancer: molecular mechanisms and therapeutic opportunities. Chem. Res. Toxicol. *30*, 1942–1955. https://doi.org/10.1021/acs.chemrestox.7b00157.

Zeman, M.K., Lin, J.R., Freire, R., and Cimprich, K.A. (2014). DNA damage-specific deubiquitination regulates Rad18 functions to suppress mutagenesis. J. Cell Biol. *206*, 183–197. https://doi.org/10.1083/jcb.201311063.

STAR★METHODS

KEY RESOURCES TABLE

REAGENT or RESOURCE	SOURCE	IDENTIFIER
Antibodies		
HRP-conjugated anti-FLAG monoclonal antibody (M2)	Sigma-Adrich	Cat#A8592
Bacterial and Virus Strains		
E. coli strain BL21(DE3)	Agilent	Cat#200131, BIL1225 (lab code)
S. cerevisiae strain BJ5464	ATCC	Cat#208288, YHU1037 (lab code)
Chemicals, peptides, and recombinant proteins		
NSC 9037: 9-Hydroxyphenylfluoron; 2,6,7-trihydroxy-9-(2-hydroxyphenyl)-3H-xanthen-3-one, $C_{19}H_{12}O_6$	NCI	N/A
NSC 80693: 9-[4-(dimethylamino)phenyl]-2,6,7-trihydroxy-3H-xanthen-3-one, $C_{21}H_{17}NO_5$	NCI	N/A
NSC 119891: 4-(3-hydroxy-6-oxoxanthen-9-yl) benzoic acid, $C_{20}H_{12}O_5$	NCI	N/A
NSC 119888: 3-(3-hydroxy-6-oxoxanthen-9-yl) benzoic acid, $C_{20}H_{12}O_5$	NCI	N/A
Fluorescein	Sigma-Aldrich	Cat#46955
NSC 157411: 6-(3-Hydroxy-6-oxo-xanthen-9-yl) cyclohex-3-ene-1-carboxylic acid, $C_{20}H_{16}O_5$	NCI	N/A
NSC 348718: 3,6-dimethoxy-9-(4-methoxyphenyl)-9H-xanthene-2,7-diol, $C_{22}H_{20}O_6$	NCI	N/A
NSC 71947: 2,7-dimethyl-9-phenylacridine-3,6-diamine, $C_{21}H_{19}N_3$	NCI	N/A
Biotinylated human ubiquitin	Boston Biochemicals/R&D Systems	UB-570
GST-tagged human ubiquitin	Juhasz et al., 2012	BIL2180 (lab code)
His-tagged human Uba1	Addgene	Cat#63571, BIL3039 (lab code)
Human Rad6B–Rad18 complex	Fenteany et al., 2019, 2020	BIL1261 (lab code)
FLAG-tagged human PCNA	Fenteany et al., 2019, 2020	BIL2366 (lab code)
Human RFC complex	Finkelstein et al., 2003	BIL2384 and BIL2385 (lab code)
Nt.BstNBI	New England Biolabs	Cat#R0607
Ni-NTA agarose beads	Macherey-Nagel	Cat#745400
Dulbecco's modified Eagle's medium	Sigma-Aldrich	Cat#RNBG1251
Fetal bovine serum	Sigma-Aldrich	Cat#26140079
Resazurin sodium salt	Sigma-Aldrich	Cat#R7017
GFP-tagged human Rad6B	This paper	BIL3293 (lab code)
GFP-tagged human Rad18	This paper	BIL3278 (lab code)
FLAG-tagged human Rad6B	This paper	BIL3097 (code code)
FLAG-tagged human Rad18	This paper	BIL3133 (lab code)
His-tagged human Rad6B	This paper	BIL3147 (lab code)
His-tagged human Rad18	This paper	BIL3181 (lab code)
Human Mms2–Ubc13	Unk et al., 2008	BIL1248 and BIL1151 (lab code)
FLAG-tagged Ubr1	Addgene	Cat#24506, RRID: Addgene_24506

(*Continued on next page*)

Continued

REAGENT or RESOURCE	SOURCE	IDENTIFIER
Critical commercial assays		
AlphaScreen FLAG (M2) detection kit	PerkinElmer	Cat#6760613
Nickel chelate AlphaLISA acceptor beads	PerkinElmer	Cat#AL108
Monolith NT.115 capillaries	Nanotemper	Cat#MO-K022
Monolith NT.LabelFree capillaries	Nanotemper	Cat#MO-Z022
Experimental models: Cell lines		
HeLa cells	ATCC	Cat#CCL-2
Recombinant DNA		
pUC19 plasmid	N/A	BIL1153 (lab code)
Software and Algorithms		
NIH ImageJ	NIH	RRID: SCR_0030
GraphPad Prism 8	GraphPad	RRID: SCR_002798
Other		
Tecan Spark microplate reader	Tecan	N/A
Thermo Scientific Fluoroskan Ascent FL microplate reader	Thermo Fisher Scientific	N/A
Heratherm IMP180 refrigerated incubator	Thermo Fisher Scientific	N/A
Monolith NT.115	Nanotemper	N/A

RESOURCE AVAILABILITY

Lead contact

Further information and requests for resources and reagents should be directed to and will be fulfilled by the Lead Contact, Lajos Haracska (haracska.lajos@brc.hu).

Materials availability

Materials are available upon request.

Data and code availability

All data reported in this paper will be shared by the lead contact upon request.

This paper does not report original code.

Any additional information required to reanalyze the data reported in this paper is available from the lead contact upon request.

EXPERIMENTAL MODEL AND SUBJECT DETAILS

Microbes

E. coli strain BL21 (DE3) (Agilent, Cat#200131) was grown in Luria-Bertani (LB) medium supplemented with the appropriate antibiotics for expression vector selection, overnight at 37°C. Transformation of the expression vectors were carried out according to the manufacturer's instructions.

S. cerevisiae strain BJ5464 cells were grown on YPD plates from glycerol stock for 1.5 days at 30 °C. Expression vectors were transformed by the LiAc transformation method (Treco and Winston, 2008). Transformant yeasts carrying expression vectors, were maintained on synthetic dropout (SD) medium lacking leucine (-leu) at 30°C.

Cell lines

HeLa cells, ATCC, Cat#CCL-2 HeLa cells were cultured in growth medium consisting of Dulbecco's modified Eagle's medium (DMEM from Sigma-Aldrich) with 10% fetal bovine serum (FBS from Gibco) in a humified cell culture incubator at 37°C with 5% CO_2.

METHOD DETAILS

Protein preparation

All proteins were of human origin except for RFC, which was of *Saccharomyces cerevisiae* origin. Flag-PCNA and Rad6-18 were overexpressed in yeast strain *S. cerevisiae* strain BJ5464, purification was followed by glutathion affinity purification, and elution was done using precision protease, while His-tagged UBA1 was purified by overexpressing it in BL21 strain, followed by Ni-affinity purification. All subunits of scRFC were overexpressed and purified from the BL21 bacterial strain. Briefly, the lysis was followed by an SP-sepharose and Q-sepharose chromatography and finished by Ni-affinity purification, using only the peak fractions in which all subunits were present. The human Rad6 used was isoform Rad6B (UBE2B). Biotinylated human ubiquitin was purchased from Boston Biochem/R&D Systems (UB-570). Anti-FLAG antibody (M2) was from Sigma. FLAG-Ubr1 was from Addgene (#24506). Fluorescein was from Sigma-Aldrich, while the rest of the compounds were from the NCI DTP. The structural integrity of the compounds was checked by mass spectrometry.

Generation of GFP-Rad6 and GFP-Rad18 fusion constructs

To generate constructs for expression and purification of mammalian green fluorescent protein (mGFP)-tagged proteins from *E. coli*, entry vectors containing human Rad6B and Rad18 cDNA sequences, respectively, were prepared. The coding sequences from these entry vectors were recombined by Gateway technology (Life Technologies) into a modified pGEX-6P-1 (Amersham) destination vector carrying N-terminal GST and mGFP tags followed by a GW cassette, prepared by the LR clonase II reaction (Thermo Fisher Scientific). For protein purification, the destination constructs were overexpressed in the *E. coli* strain BL21(DE3) codon+ (Agilent). First, expressed proteins were purified as GST fusion proteins with glutathione agarose beads (Thermo Fisher Scientific). The GST moiety was removed with PreScission protease (GE Healthcare) resulting in mGFP-tagged proteins.

Alpha assays

Alpha beads were procured from PerkinElmer for the Alpha assays, which are based on the luminescent oxygen channeling immunoassay and were licensed to PerkinElmer. There are two varieties of the Alpha assay (both of which depend on excitation at 680 nm), AlphaScreen and AlphaLISA, which only vary in the fluorophores used in the acceptor beads (anthracene and rubrene for AlphaScreen, with emission maximum at 520-620 nm, or a europium chelate for AlphaLISA, with emission maximum at 615 nm), while the donor beads are the same in both assays. We used AlphaScreen acceptor beads in the experiments described in this paper. Unless otherwise noted, the donor beads were coated with streptavidin, while the acceptor beads were coated with anti-FLAG antibody. Plates for screening and follow-up Alpha experiments were read in a Tecan Spark plate reader equipped with a dedicated laser for excitation in Alpha assays, plate stacker, and heating and cooling module for precise temperature control. All Alpha assays were carried out in 96-well white round-bottom polypropylene plates (Greiner) at 25°C.

PCNA ubiquitination

To assay for overall PCNA ubiquitination, reactions were conducted in a buffer of 40 mM Tris, pH 7.5, 8 mM $MgCl_2$, and 10% glycerol (reaction buffer) with 150 nM biotinylated ubiquitin, 50 nM FLAG-PCNA, 10 nM RFC, 2 nM nicked pUC19 DNA, 50 nM Uba1, and 100 nM Rad6–Rad18. Following preincubation for 15 min with each compound (or DMSO solvent alone), reactions were initiated by addition of ATP to 100 μM, with incubation for 2 h at 25°C, followed by tenfold dilution in a buffer of 25 mM HEPES, pH 7.5, 100 mM NaCl, 0.1% Tween 20, and 1 mM DTT (Alpha buffer) containing 20 mM ethylenediaminetetraacetic acid (EDTA) and streptavidin donor and anti-FLAG acceptor AlphaScreen beads, both at 10 μg/ml, unless otherwise noted, under low-light conditions with dark yellow-green filter (LEE 090) covering sources of lighting. The reaction step was terminated at the time of addition of the Alpha buffer containing EDTA to chelate the Mg^{2+} from the ATP-Mg^{2+} required for both PCNA loading by RFC and Uba1 charging with ubiquitin. The samples in Alpha buffer with beads were incubated for 4 h at 25°C (which we previously

found is an optimal time for yielding strong signals (Fenteany et al., 2020)) and then read by the plate reader.

Uba1∼ubiquitin thioester formation

The reactions were conducted in reaction buffer containing 50 nM FLAG-Uba1 and 150 nM biotinylated ubiquitin. Compounds (or DMSO alone) were added, and samples were incubated for 15 min at 25°C. The reactions were initiated by the addition of ATP to 100 μM, then incubated for 30 min at 25°C, followed by termination and tenfold dilution of the reactions in Alpha Buffer containing 20 mM EDTA (DTT was omitted here from the Alpha buffer to avoid cleavage of the thioester bond in this and the Rad6∼ubiquitin thioester formation reaction). The donor and acceptor beads in the buffer were at 10 μg/ml. After 4-h incubation at 25°C in the dark, the plates were read by the plate reader. For gel-based confirmation, similar reaction conditions were used except for 150 nM FLAG-Uba1 and 450 nM GST-ubiquitin (GST was used as a tag to ensure clear resolution of Uba1∼ubiquitin from free Uba1), with visualization by silver staining.

Rad6∼ubiquitin thioester formation

For initial precharging of Uba1 with biotinylated ubiquitin, 100 nM His_6-Uba1 was combined with 300 nM biotinylated ubiquitin in reaction buffer, with reactions initiated by the addition of ATP to 100 μM, followed by incubation for 30 min at 25°C, at which time EDTA was added to 20 mM to quench further charging of Uba1 with ubiquitin, which is the only step in these two sequential reactions that requires ATP-Mg^{2+}. The samples were then combined with an equal volume of 100 nM FLAG-Rad6 in reaction buffer, which had been preincubated with each compound (or DMSO alone) for 30 min at 25°C. The samples were then diluted tenfold in Alpha buffer (omitting DTT) containing 20 mM EDTA, with donor and acceptor beads at 10 μg/ml. After 4-h incubation at 25°C in the dark, the plates were read by the plate reader. For gel-based confirmation, similar reaction conditions were used except that 300 nM FLAG-Uba1, 1 μM FLAG-Rad6, and GST-ubiquitin were used, with visualization by silver staining.

Rad18 autoubiquitination

50 nM His_6-Uba1 was precharged with 100 nM biotinylated ubiquitin in reaction buffer by adding ATP to 100 μM, followed by incubation for 30 min at 25°C. 100 nM FLAG-Rad18 and 100 nM Rad6–Rad18 complex, 100 nM FLAG-Rad18 and 100 nM Rad6 in reaction buffer were preincubated with each compound (or DMSO alone) for 15 min at 25°C. The Uba1 charging reaction was quenched by addition of EDTA to 20 mM. The two samples were then mixed 1:1 and incubated for 1 h at 25°C, followed by tenfold dilution in Alpha buffer containing 20 mM EDTA, with donor and acceptor beads at 10 μg/ml. After 4-h incubation at 25°C in the dark, the plates were read by the plate reader.

Rad6–Rad18 interaction

A solution of 100 nM FLAG-Rad6 and 100 nM His-Rad18 was incubated for 30 min at 25°C in reaction buffer, then each compound (or DMSO alone) was added with incubation for 30 min at 25°C. After tenfold dilution in Alpha buffer with nickel chelate donor beads and anti-FLAG acceptor beads, both at 10 μg/ml, and 4-h incubation at 25°C in the dark, the plates were read by the plate reader.

Mms2–Ubc13∼ubiquitin thioester formation

For initial precharging of Uba1 with ubiquitin, 300 nM FLAG-Uba1 was combined with 1 μM GST-ubiquitin in reaction buffer, with reactions initiated by the addition of ATP to 100 μM, followed by incubation for 30 min at 25°C. The charging of Uba1 with ubiquitin was quenched by the addition of EDTA to 20 mM. The samples were then combined with an equal volume of 1 μM Mms2–Ubc13 in reaction buffer, with the samples having been first preincubated with each compound (or DMSO alone) for 30 min at 25°C. Detection was performed by silver staining.

Microscale thermophoresis

Microscale thermophoresis was performed with a NanoTemper Monolith instrument. The compound was serially diluted and incubated with 20 nM of GFP-Rad6 or GFP-Rad18 for 15 min. The samples were loaded into capillaries, and the NanoTemper Monolith software was used to determine the K_d.

Rad6–Ubr1 pull-down

Equimolar GST-Rad6 and FLAG-Ubr1 (1 μM) were mixed and incubated with the compound for 15 min at 25°C and then loaded onto an affinity chromatography column containing glutathione-agarose beads. Elution was done with 20 mM glutathione and visualization by silver staining.

Rad6–Ubr1 interaction alpha assay

Equimolar GST-Rad6 and FLAG-Ubr1 (100 nM) were mixed and incubated with the compounds for 15 min at 25°C in reaction buffer, followed by dilution by a factor of 10× in Alpha buffer, with donor and acceptor beads at 10 μg/ml. After 4-h incubation at 25°C in the dark, the plates were read by the plate reader.

Cell culture

HeLa cells were cultured in growth medium consisting of Dulbecco's modified Eagle's medium (DMEM from Sigma-Aldrich) with 10% fetal bovine serum (FBS from Gibco) in a humified cell culture incubator at 37°C with 5% CO_2.

Cell survival

HeLa cells were plated onto 96-well cell culture plates at a density of 1×10^4 cells in 50 μl per well in DMEM containing 0.5% FBS at 37°C and 5% CO_2. Compounds (or DMSO alone) were added 24 h later. After another 24 h in the presence of compounds, resazurin (Alamar Blue) was added. Color change was measured 4 h later on a fluorescence plate reader with excitation of 570 nm and emission of 585 nm.

Computational docking of compounds to Rad6

The nuclear magnetic resonance solution structure of the full-length human Rad6B (PDB ID: 2Y4W) (Huang et al., 2011) was retrieved from the Research Center for Structural Genomics Protein Data Bank. The ten lowest energy structures published were used as docking targets. Parallel blind dockings were performed using the Autodock 4.2 software, and Lamarckian genetic algorithm was run with default parameters from AutoDock 4.2. The maximum of energy evaluations was set to 2,500,000. Dockings were performed in two overlapping 90.0 Å × 124.0 Å × 90.0 Å grid volumes, large enough to cover the whole molecular surface of Rad6B. Consequently, the whole surface of the protein was probed for potential binding sites without any *a priori* knowledge or artificial bias. The spacing of grid points was set to 0.375 Å. All ligand torsions were kept flexible during dockings. Although protein coordinates were kept rigid, internal flexibility of the protein was partially accounted for by docking to 10 different, experimentally derived structural states. 1,000 dockings were performed for each target and grid with the above settings resulting in an ensemble of 20,000 Rad6–NSC 9037 complexes. These complexes were then clustered using a tolerance of 2.0 Å and ranked according to the corresponding binding free energies. *In silico* inhibitory constants were calculated from binding free energies derived from docking, according to the following equation: $\Delta G = RT \ln K_i$. Selected high-affinity binding poses were subjected to further contact analysis. Potential binding poses were selected on the basis of predicted binding affinities and apparent site specificity. Low affinity surface-bound poses were omitted. 4–14 high-affinity binding poses were selected for each of the 10 Rad6B structural states, which were then subjected to further contact analysis.

A second series of refined flexible blind dockings was performed using a single Rad6 target structure, selected on the basis of pilot blind dockings. This was extended to include all of the compounds. Furthermore, amino acid side chains which were found in the pilot dockings to frequently participate in protein–ligand interactions were kept flexible in the second series (Table 2), providing 18–32 torsional degrees of freedom during the respective dockings. All oter docking parameters were the same as above. K_i values were derived from the binding free energies and specific residues of contact were determined for these refined binding poses, as listed in Table 2.

QUANTIFICATION AND STATISTICAL ANALYSIS

GraphPad Prism 8 and Microsoft Excel was used to calculate all the IC50 and curve fitting calculations. Statistical parameters used for the analysis.Signal-to-noise (S/N) and Signal-to-background (S/B) = They are indication of the degree of confidence with which signal can be regarded as real.

$$S/N = \frac{\text{mean signal} - \text{mean background}}{\text{standard deviation of background}}$$

$$S/B = \frac{\text{mean signal}}{\text{mean background}}$$

z-factor: The z-factor is defined in terms of four parameters: the mean and standard deviation of both positive and negative controls.

$$Z = 1 - \frac{3\text{SD of sample} + 3\text{SD of control}}{\text{mean of sample} - \text{mean of control}}$$

Strictly standardized mean difference (SSMD) and Signal window values: It is the mean divided by the standard deviation of the difference between two random groups, on the other hand signal window value is more indicative measure of the data range in the HTS assay.

Statistical details can be found in the figure legends.